UNIVERSITY OF NAIROBI

MAPPING RADIOACTIVE MINERALS USING REMOTE SENSING: A CASE STUDY OF MRIMA HILL KWALE COUNTY, KENYA

By

Jephter Ongige Ondieki

S56/78901/2015

Bsc-Astronomy

A Thesis Submitted in Partial Fulfillment of The Requirements for award of the Degree of Master of Science in Nuclear Science of The University of Nairobi.

November 2020

i

Declaration

I declare that this thesis is my original work and has not been submitted elsewhere for examination, an award of a degree or publication.

Signature…………………………….. Date……………………………………

Jephter Ongige Ondieki.

S56/78904/2015

Institute of Nuclear Science and Technology

University of Nairobi

This thesis is submitted for examination with our approval as research supervisors:

Mr. Michael J. Mangala   Signature   Date
Institute of Nuclear Science   ……………....................   ………………………………
University of Nairobi
P.O. Box 30197-00100
Nairobi

Prof. Collins O. Mito   Signature   Date
Department of physics   ……………....................   …………………………
University of Nairobi
P.O. Box 30197-00100
Nairobi

Dr.Geoffrey O. Okeng'o   Signature   Date
Department of physics   ……………………………   ……………………………
University of Nairobi
P.O. Box 30197-00100
Nairobi

Prof. Ayub Gitau
Dean School of Engineering   Signature   Date
      ………………………   ………………………………..
University of Nairobi
P.O Box 30197-00100
Nairobi

Dedication

To my late dad and my late sister for all their guidance they provided me throughout my life. Rest in peace Dad and sister Hyline.

Acknowledgment

First, I would like to thank my Lead supervisor, Mr. Michael Mangala for his fundamental support to the completion of this thesis. His insights, encouragement, and ability to keep me on the track were helpful throughout the duration of this work. He has always provided me with useful advice and comments on how best, to improve my work. Thank you for your patience and encouragement. Also, I would like to thank my other supervisors; Prof Collins O. Mito, Prof Ayub Gitau and Dr Geoffrey O. Okeng'o for their inputs and suggestions to improve this work.

Second, I appreciate the generosity of Dr.Ian Kaniu, for providing me with the radiometric data of the study area. Thank you so much, sir. I acknowledge with thanks, the Nuclear Power Energy Agency (NUPEA), formerly Kenya Nuclear Electricity Board (KNEB), for awarding me a scholarship which enabled me to do the Nuclear Science program at the University of Nairobi.

Special thanks to the late David Maina, the former Director, Institute of Nuclear Science and Technology for being a great source of inspiration and a fountain of knowledge. Rest in peace sir, I will miss your guidance. Very special thanks to the entire staff and students of the Institute of Nuclear Science and Technology, for their team spirit and assistance. And last, I am grateful to my parents for their support and encouragement. Without their constant encouragement, it would not have been possible to finish this work. I would like to thank my brothers and sisters as well, for their support.

Table of Contents

List of Tables

List of Figures

List of Abbreviations and Acronyms

ASTER   Advanced Space borne Thermal Emission and Reflection Radiometer

AVIRIS	airborne Visible/Infrared Imaging Spectrometer
DN	Digital Number
ETM+	Enhanced Mapper Plus
FCC	False Color Composite
FLAASH	Fast Line-of-sight Atmospheric Analysis of Hypercubes
GIS	Geographic information System
IRS	Infrared Sensor
MLC	Maximum Likelihood Classification
MNF	Minimum Noise Fraction
MTMF	Mixture Tuned Matched Filtering
MSS	Multispectral Scanner Sensor
NDVI	Normalized Difference Vegetation Index
NIR	Near Infrared
OLI	Operational Land Imager
PCA	Principal Component Analysis
PC1	Principal Component 1
PC2	Principal Component 2
PC3	Principal Component 3
PC4	Principal Component 4
PC5	Principal Component 5
PC6	Principal Component 6
PC7	Principal Component 7
RGB	Red Blue Green
ROI	Region of Interest
SAM	Spectral Angle Mapper
SWIR	Short Wave Infrared
Th	Thorium
TIRS	Thermal Infraared Sensor
TM	Thematic Mapper
PIMA	Mineral Analyzer

USA   United States of America

VNIR   Near Infrare

Abstract

Mrima hill is an elliptical carbonatite plug area of approximately 2 km across, a gazetted forest reserve in Kwale county, bounded by 4° 29'l0"S; 39° 15 '10'' E coordinates, 750 feet above the sea level. The hill is covered by deeply weathered materials. Rare earth elements, niobium, Monazite minerals and associated carbonatite rocks are known to exist in the area. The area is classified as a high background radiation. Applications of geological remote sensing and GIS for radioactive mineral mapping have not been fully integrated into the mineral exploration activities of the Geological Survey of Kenya. This study employed remote sensing and Geographic Information System (GIS) to map minerals in Mrima hill region in Kwale County, specifically radioactive minerals, as the area has been classified a high background radiation area. In this study, the data used was obtained from Earth explorer (https://earthexplorer.usgs.gov/) website, with spatial resolution of 30 m, and was processed for mineral spectral signatures by using ENVI5.3 and Arc Map 10.3 software by means of the color composite, band rationing, principal component analysis and supervised classification.Landsat-8 OLI imagery of Mrima hill was processed to enhance the geological features and mineral potential of the area. Band ratios 6/7, 6/5, 4/2 were assigned to RGB. Band ratio 4/2 highlighted ferric ion minerals, 6/5 emphasized ferrous minerals, and 6/7 distinguished iron oxide minerals from carbonate minerals. In a second technique, band ratio 6/7 was replaced with 7/ 5 in order to accentuate clay minerals with high reflectance within band 7. Supervised classification training data were obtained using five classes for rocks associated with radioactive minerals (carbonatite, granites, sandstone, serpentine and shale). The classification using maximum likelihood classification was fairly accurate and matched the radiometric and geologic map of the area, also showing an alteration zone that coincided with the high dose rate areas. However, for areas covered by vegetation, botanical indicators of vegetation species associated with radioactive mineralization including, the *Asparagus sp, Stanleya, Aster venustus, and Oryzopsisj* species, from the Envi database, were used to map for the presence of radioactive minerals in the study area. The use of supervised classification method identified the following vegetation; big berry Manzanita, big sagebrush, Mormon tea, pynon pine, specifically as associated with radioactive minerals. The classified image was finally validated using existing radiometric data of the study area. In conclusion, this study demonstrated the usefulness of applications of remote sensing to map minerals in general, for application in mineral exploration.

Chapter One: Introduction

1.1   Background

Majority of developing Nations depend on minerals to sustain their economies. Prior information of minerals occurrence, including their location maps and the geology of an area, is very useful for the exploration purposes. However, this requires a lot of investments in terms of time, money and even labor for exploration, especially in remote inaccessible areas. In this case therefore, the use of remote sensing not only for geological purposes, but also to be available to potential investors for the purpose of mineral exploration is necessary(Rokos *et al*, 2000). In practice, remote sensing has the advantage of reducing the risks for investors in the mining sectors (Drury, 2001)

Remote sensing was used earlier, for the mapping of vegetation only, this is as a result of the sensors being designed for vegetation mapping only. (Langley *et al*, 2001; Jung *et al*, 2006). The reflectance of vegetation is high in the near infrared and high absorption in the red wavelength of the electromagnetic spectrum. Their comparison gives the status of the vegetation in an area.

For mineral mapping, specific vegetation species are also used as indicators, for example, radioactive minerals, they include; big berry Manzanita, Mormon tea, and sagebrush are good absorbers of selenium and gypsum. In general, selenium and gypsum are found in uranium ores deposits, therefore, this vegetation are also used to indicate the presence of radioactive minerals.

During the exploration of minerals, ground mineral mapping, depends on the data derived from the field and also on the laboratory tests of sampled specimen. The data from these fields is then analyzed for geological information. The use of remote sensing technology may not replace the level of accuracy, but however, provide information which is more cost effective, and the use of this technology, in areas which may not be accessible during ground explorations (Rajesh, 2004).

In Kenya, the mineral deposits occur in different geological settings. Some deposits are associated with Paleocene rocks such as fluorite, diatomite, oil, gas, barite etc. Others are associated with Achaean craton such as gold, copper and nickel. Most of these deposits which are located within the Kenyan Neoproterozoic Mozambique belt have not been adequately studied. In order to study these mineral deposits more effectively, it is important to subdivide them to categories. The subdivision is based on several criteria such as the kind of mineral or

metal contained in the host rock or the shape or size of the deposits. Evans (1993) has classified mineral deposits into (1) mineral deposits that originate due to internal processes i.e. magmatic segregation, hydrothermal, lateral secretion and metamorphic processes; and (2) mineral deposits that originate due to surface processes i.e. mechanical accumulation, sedimentary precipitates, residual processes, secondary supergene enrichment and volcanic exhalative deposits.

The coastal region of Kenya has been of most concern to researchers as a region of high background radiation. Mineralization studies conducted in the area such as the one by the Austromineral in collaboration with the Kenyan government found out the area to contain sediments having zircon ore and some concentrations of radioactive isotopes such as lead and zinc (Austromineral, 1978). Areas around Mrima hill and Jombo were found to contain rare earth metals and niobium. Gamma radiation levels are high around Mrima hill in addition to the cosmic content (Patel 1991a & b). This may expose the residents to high radiation beyond the world average limit of 2.4 mSv annually. A report by the radiation board of Kenya indicated patterns of high radioactivity in some areas of the south coast due to high levels of radiation from Mrima hill and this confirm the results by Patel (Patel, 1991b).

Mrima hill is one of the regions with the highest level background radiation with some areas reporting external gamma exposure levels as high as 108 mSv/y (health research foundation, 2000). These exposures are attributed to the radionuclide in the decay chain of 232Th and to some extent 238U. The geology of Mrima hill is characterized by carbonatite rock formation, which is generally associated with elevated concentration of 232Th. Besides, monazites and zircon, which naturally contain trace amounts of 238U and 232Th as well as phosphate ores commonly associated with radionuclide in the 238U decay series, are known to exist (Achola, S.O, 2009).

Granite rocks are the possible source of uranium and thorium deposits and therefore the study of granites are important in identifying the candidate sites of these radioactive minerals. The following are the rocks which are associated with radioactive minerals; granite, basalt, biotite, limestone, sandstone, shale, bedded phosphate and coal rocks. However, radioactive minerals are rarely found in basalt, limestone, bedded gypsum, quartzite, and marble rocks.

Uranium mineralization are also found in felsic igneous rocks, ferric iron and faulting. Hence, for the prospection of uranium, these geological features are employed. In areas such as Mrima

hill, the use of field work is impractical since these regions are inaccessible. The use of remote sensing use low spatial and spectral resolution data which enable mapping of minerals in inaccessible regions thus enables low cost of collection of data.

The use of remote sensing in geological applications requires more spectral bands and smaller bandwidth. The information about minerals and rocks are found in the middle or shortwave and to some extent the thermal region of the spectrum than on the visible band.

Multispectral sensors are useful when carrying out mineral mapping, for example, the shortwave Infrared bands on Landsat Thematic Mapper 5 and 7 are useful when carrying out discrimination between different types of minerals and rocks. This has led to the use of thematic mapper sensor of Landsat satellite in identifying different lithologies (Loughlin, 1991; Liu, 2007). Sensors such as ASTER have been used in discrimination of minerals and rocks. (Crosta and Filho, 2003).

In general, metallic minerals are hosted in basement rocks and include occurrences of; gold, platinum, rare earth metals, zinc, iron, nickel while industrial minerals are hosted in Precambrian rocks. One of the important sources of uranium is granite rocks. There is relatively high concentration of uranium and thorium in these rocks as compared to other rocks (Pavlidou *et al*, 2006).

Therefore, using remote sensing has led to better understanding of naturally occurring radioactive minerals in terms of qualitative and quantitative analysis of minerals in applications in characterization of the geology for mineral content. This is because it provides information on rocks types which are found on the earth's surface and its mineralogy. The interaction of rocks with electromagnetic radiation results in unique response for each rock. These results to unique spectral response for each mineral thus different mineral have a different spectral response. This can be discriminated from other rocks by the use of various image processing techniques and image classification techniques (Loughlin, 1991; Sabins, 1999; Kusky and Ramadan, 2002; Crosta and Filho, 2003; Gabr, 2010).

This study was aimed in mapping radioactive minerals in Mrima hill, Kwale County, by the use of various remote sensing techniques, using their indicators; such as identifying the parent rock formations and botanical vegetation species associated with radioactive minerals.

1.2   Problem statement

To map bedrock and identify presence of specific diagnostic minerals, it is possible to use remote sensing methods. Remote sensing is an additional tool for geologist to understand the overall lithological of an area and to define potential exploration target (Floyd F. Sabins 1986).

The exploration of minerals usually requires intensive fieldwork for the purpose of knowing better the features associated with geology of the study area. Geological maps of the study areas provide useful datasets such that these maps help in focusing the exploration efforts in areas. The maps can also be used when planning land use and also predicting future explorations (Boleneus *et al.* 2001). Radioactive minerals pose great hazards because of their decay which emits harmful ionizing radiations. The degree of hazards, depends on their concentrations, the energy of radiations being emitted and the type of radiation or proximity to the organs of the body.

In Kenya, there is insufficient use of modern mapping methods such as remote sensing for exploration of large areas to map promising zones for more detailed studies by ground follow up. So far, all the previous studies in the study area have been done using field exploration methods. It is hypothesized that remote sensing can be useful in geological mapping and exploration for rocks associated with radioactive minerals. Many common rocks forming mineral can be detected by remote sensing because they have diagnostic spectral signatures that allow mineral species identification.

1.3 Justification and Significance of the Study

Mrima hill has been classified as high radiation background area. However, most studies in the area have been conducted by field exploration. In particular, Patel and Mangala (1994) associated these high levels of radiation dose rate with the occurrence of thorium and uranium, while Patel (1991) associated, with presence of carbonatite rocks in the area.

In most developing countries like Kenya, most of the geological studies such as minerals exploration are mostly done by field work. There is very little deployment of the aerial satellite mapping techniques for mineral exploration. The use of satellite technology in mapping the geology and also in mineral exploration is cost effective as it has been demonstrated elsewhere

and can be used in areas which are inaccessible (Rokos *et al...*2000). Also, these data can be incorporated with other database because of its digital nature.

The study is expected to map potential mineralization zones in the study area.

1.4   Objectives
1.4.1   Overall Objective

The overall objective of this study was to use remote sensing and Geographical Information System (GIS) techniques to map potential radioactive mineral areas in Mrima hill, Kwale County, Kenya.

1.4.2   Specific Objectives

   a) Map rock types, mineral alteration, vegetation types and structure by use of Landsat data of the study area from Earth Explorer website (http://www.earthexplorer.usgs.gov/).
   b) Delineate potential sites of radioactive minerals.
   c) Validate remote sensing results by the use of existing radiometric survey data of the study area.

1.5   Scope and limitations of the study

Mrima hill is located in Kwale county Kenya bounded by 4° 29'l0"S; 39° 15 '10'' E coordinates. The hill rises to a height of approximately 750 feet above the coastal plain. It forms an elliptical carbonatite plug of approximately 2km across. The hill is covered by deeply weathered materials. The region has been previously, explored for niobium and rare earth elements (Coetzee and Edwards, 1959). There are reports of phosphates that occur in form of monazite and barium phosphate mineral being reported in the area. Also minor amounts of apatite have been reported in the area (Coetzee and Edwards, 1959). The soil of the area is mainly red loam though some parts have clay type of soil.

According to (Patel, 1991), the area is described as a high natural background radiation area. Elemental analysis of carbonatite rock samples has shown elevated levels of thorium (Patel and

Mangala, 1994).The main economic activities are subsistence farming. A significant portion of the study area is a government gazetted forest reserve.

This study was limited to the use of the spectral data of the rocks and vegetation species available in ENVI 5.3 database, in identifying the rock formation lithology and vegetation species associated to radioactive minerals occurrence. The data used was Landsat 8 obtained on the 30th March, 2016.

The results of this study were validated by the use of existing radiometric data of the study area (Kaniu, 2018).

Chapter Two: Literature Review

2.1   Introduction

Remote sensing is defined as the process of obtaining information about material of interest without being in physical contact with the material. The process involves analyzing the data acquired (Lillesand, 1999).

The resulting imagery needs to be processed further and interpreted to give out useful information. This information can be useful in various sectors of economic development such as; agriculture, forestry, environment, and geography. Remote sensing is also useful in development projects; such construction and built industry, urban planning, land surface survey, etc. The aim is to find out information related to natural resources data on the earth's surface (Lo *et al*, 1997).

2.2   Remote Sensing for Geological mineral mapping

Remote sensing techniques help in mapping of geology of an area therefore helping in mineral exploration. The localization of ore deposit is achieved by using the unique spectral response of the various minerals and rocks.

The geological mapping by the use of remote sensing requires more spectral bands and smaller bandwidth in the electromagnetic spectrum. The information about minerals and rocks are found in the middle or shortwave and to some extent the thermal region of the spectrum than on the visible band.

Satellites have been in continued launching starting with the launch of Landsat 1 in the year 1972. In following years i.e. 1975, 1978 and 1982, Landsat 2, 3 and 4 were launched respectively. These satellites were operating in the near orbit. They carried the Multispectral Scanner Sensor with exception of Landsat 4 and 5 which had the thematic sensor and the multispectral scanner sensor. They were used to detect radiation reflected from the surface of the earth in the wavelength region comprising the visible and infrared bands. Table 2.1 shows the Landsat Multispectral Scanner Sensor and its primary use (source: www.usgs.gov).

Table2.1: Landsat 1-3 and Landsat 4-5 Multispectral Scanner Sensor and spectral bands and their applications. (Source: www.usgs.gov)

Band designation in Landsat 1,2 and 3	Band designation in Landsat 4 and 5	Spectral range(μm)	Application
4	1	0.5-0.6	Sediment-laden water delineates areas of shallow water
5	2	0.6-0.7	Cultural features
6	3	0.7-0.8	Vegetation boundary between land and water and landforms.
7	4	0.8-1.1	Penetrates atmospheric haze best, emphasizes vegetation, the boundary between land and water and landforms.

The launch of Landsat 7 was done April 1999 and on it carried the ETM+ sensor. It has eight bands which are the visible bands through to panchromatic bands. Landsat 7 has a scene size of 170km by 185km. It provides all radiometric and geometric calibration needed in processing raw image data.

Table 2.2 shows the Thematic Mapper and Enhanced Thematic Mapper plus sensors in Landsat 4-5 and Landsat 7 and their applications in remote sensing.

Table2.2: Landsat 4-5 Thematic Mapper and Landsat 7 Enhanced Thematic Mapper plus spectral bands and their applications (source: www.usgs.gov)

Bands	Spectral range(μm)	Useful for mapping
1	0.45-0.52	Differentiating soil from vegetation,
2	0.52-0.60	Mapping plant vigor or health
3	0.63-0.69	Used for discriminating vegetation slopes.
4	0.77-0.90	Shoreline mapping
5	1.55-1.75	Soil moisture content mapping
6	10.40-12.50	Used for Thermal mapping
7	2.09-2.35	Mapping of altered rocks and mineral deposits
8(Landsat 7 only)	0.52-0.90	15m, sharper image definition

On the 11th Feb 2013, the Landsat 8 satellite was launched containing two sensors on board i.e. the operational land imager (OLI) and Thermal Infrared (TIRS) sensors on it. The OLI sensor has nine spectral bands which range from visible through panchromatic to cirrus. The TIRS has two spectral bands. Landsat 8 has a scene size of 170km by 185km.

The table 2.3 summarizes the spectral bands of Landsat 8 and their application.

Table2.3: Landsat 8 spectral bands and their applications (source: www.usgs.gov)

Bands	Spectral range(µm)	Useful for mapping
1	0.43 - 0.45	Aerosol mapping
2	0.45-0.51	Mapping vegetation and soil
3	0.53 - 0.59	Mapping plant vigor
4	0.64 - 0.67	Distinguishing vegetation slopes
5	0.85-0.88	Shoreline mapping and biomass
6	1.57 - 1.65	Moisture content in soil and vegetation
7	2.11 - 2.29	Alteration mapping of rocks
8	0.50 - 0.68	15-meter resolution, image delineation
9	1.36 - 1.38	Improved mapping of cirrus clouds
10	10.60 – 11.19	Soil moisture thermal mapping
11	11.5 - 12.51	Soil moisture thermal mapping

Hekmati (2001) used ASTER data together with geological reports and maps in mapping uranium minerals in Northern Iraq. In his work, the ASTER data were processed using the ERDAS imagine v.9.1 software and Arc Gis v.9.1. He established that the area had high to medium radioactive minerals.

Liu *et al* (2011) used ETM+ sensor in mapping gold minerals in the arid and semi-arid region of Shandong Province China. In his study, he used masking techniques to suppress the effects of vegetation and clouds cover and used Crosta techniques to identify gold minerals.

Soe *et al* (2005) used ASTER and Landsat TM data in the mapping of iron oxide in the Tanintharyi coastal area, Southern Myanmar. The minerals were mapped by the use of color composite techniques in the area of interest.

Hydrothermal zones have been identified using ASTER satellite data in Nevada USA. The zones are associated with copper and gold minerals. The techniques applied included; the use matched filtering method which identified the distribution of the alteration zones (Pour and Hashim 2012a). It was found out that the use the spectral reflectance gives good results in terms

of the mineral ore deposit. The rocks were identified in zones such as the argillized, a silicified and an opalized zone.

Dogan (2008) used remote sensing and GIS in Tokat province in Turkey to map different minerals such as ferrous and iron oxide minerals. He used Landsat- ETM$^+$ satellite images. NDVI was applied in mapping vegetation in the study area and the product masked out to avoid the incidence of wrong interpretation. Mapping of the ferrous and iron oxide minerals were done by applying the various remote sensing techniques in the study area.

The use multispectral data were used in mapping of magnetized quartzite in Tamil Nadu coast (Chandrasekhar*et al*., 2001). In this study he identified end members by and compared it with the spectral library obtained from the United States Geological Survey (USGS) spectral library. The end member was mapped by the use of the Spectral Angle Mapper technique. The accuracy of the results was done by carrying out ground survey and it was found out that the results were in agreement with the obtained results.

Mapping of silicate and carbonates rocks has been done by the use of ASTER data (Yamaguchi et al., 1998). The capability of the sensor in ASTER in discriminating various rocks has been proved by several studies (Abdeen et al., 2001; 2002; Alimohammadi *et al*., 2015; Amer *et al.,* 2010). Various mining companies and geologist have used the applications for exploration.

Wen and Han (2009) mapped copper deposits in Southwest China by the integration of data sets into a GIS and analyzed using the Arc-SDM software. Geophysical, geochemical Data, satellite datasets and deposits training data were used for the analysis. The use of evidence model was then used to generate the potential mapping region for cost-benefit exploration and characterization of such economic important minerals, ore deposits, and rock types

2.3   Mineral Mapping using Remote Sensing Applications Techniques

Mapping is a technique used in showing location with abundance of certain materials and produce maps of the same. Various methods have been used to discriminate the various rocks and minerals deposits by the use ASTER data. The methods include the use of spectral angle mapper, false color composite (Rajendran *et al*., 2013a; 2014; Rajendran and Nasir, 2015a), band ratios (Rajendran *et al.,* 2012; Rajendran and Nasir 2014a; 2015b) and principal components

analysis (Rajendran 2016; Rajendran and Nasir 2015a; Rajendran *et al.*, 2011; 2012; 2013a; 2014).

2.3.1 Band Ratio and Color Composite applications

Increasing the contrast between bands and reducing effects due to topography, requires the use of band ratio technique. It is provided for by dividing one band by another. Huizhou (2013) used ASTER data in mapping minerals. In order to carry out discrimination of rocks in the area of study, the use color composite, band ratio, and principal component analysis were used to study the tectonic structure of the study area. Prospective maps were produced by the use of weighted overlay and logistic regression models. From the result, it showed that ASTER data was useful in mapping the alteration zones, where radioactive minerals are present as compared to non-mineralized areas.

The algorithms proposed by Cardoso Fernandes *et al* (2019) were applied to evaluate potential exploration of Li pegmatite occurrence by Santos *et al* (2019) in the pegmatite filed of São João Del Rei in Brazil. He used the techniques of band ratio and selective principal component analysis. The results showed that Li pegmatite was more accurate in São João than in Araçuaí, because the vegetation cover in the area negatively influenced the results as reported by Santos *et al* (2019). In the study area, the successful band ratio was the one as proposed based on the reference spectrum of lepidolite Li-bearing mica: Landsat-5 3/7, Landsat-8 4/7 and Sentinel-2 4/7 Cardoso Fernandes *et al* (2019) .In general, the selective PCA presented the most accurate results as compared to the band ratio technique Santos *et al* (2019). Nevertheless, the results obtained were very significant, contributing to the state of the art of this field, since not only did it confirm the methodology proposed by Cardoso-Fernandes *et al* (2019) but also showed its ability to detect other pegmatite occurrences with Li potential besides the known target areas. Currently, field validation is in progress to check if Li mineralization is in fact present in the potential areas identified

Ramadan *et al* (2013) used ETM+ of Landsat in exploring Uranium deposits by applying to it various remote sensing techniques using the ERDAS 8.3 software. The data obtained was processed by the use of false color composite and band ratio. The band ratio was used in discriminating different types of rocks and density slicing was used to convert the gray scale

images to the digital number. In the study, the ratio, 5/7 was applied in mapping clay alterations. Supervised classification was then used to identify the alteration zones. Processing Landsat images distinguished between different rocks and between alteration zones and non-mineralized zones. The presence of Uranium-bearing zones was found by carrying out the correlation of Uranium contour map and the band ratio images.

Griffiths *et al* (1987) carried out Uranium mineralization using Landsat data and other satellite imagery for the generation of geological maps with structural and lithological information. The Landsat images were processed using false color composite, band ratio and the use of fieldwork. The image geological maps were completed based on the interpretation of the Landsat MSS and Red Blue Green (RGB) imagery as well as fieldwork. During fieldwork, some other minor minerals were observed and those which were most significant were observed in the low-grade metal sedimentary and metavolcanic rocks.

Mshiu (2011) used Landsat 7 data to study the different rocks in Rongwe province in Tanzania. Landsat data was processed by the application of band ratio which is used for discriminating different rocks as different rocks have different spectral signatures. The color composite images clearly distinguished different rocks in the study area as it discriminated individual lithological units in the different rocks in the study area.

Mineral exploration in Wadi Bidah mineral district in Saudi Arabia was explored by the use ASTER and ETM[+] data (Volesky *et al*, 2003). Remote sensing data together with GIS were used to map out the lithology and mineral deposit areas. They used color composite images and band ratio to map the sulfide deposit area. The results indicated the presence of sulfide deposits rich in iron and hydrothermal areas all having unique spectral signatures.

The use band ratio of 4/7, 4/6 and 4/10 using ASTER data were used to map lithological areas in Sinai, Egypt (Gad and Kusky 2007). Maps of the rock units were produced which consisted of iron formation rocks, granites volcanic rocks and migmatite.

2.3.2 Principal Component Analysis applications

The use of the PCA together with band rationing and edge enhancement techniques in image processing was used to determine Uranium-bearing dolomites (Raghu *et al,* 1989). The image

data were digitally co-registered with the survey data using the ERDAS software. The interpretation of the satellite data Infrared Sensor (IRS) P6 LISS was carried out to delineate various landforms categories in conjunction with the survey data using the ERDAS software. Selected image subsets were prepared and supervised and unsupervised classification methods were applied to map various rocks in the study area using their spectral reflectance. Granite rocks were found to be source of Uranium in the study (Shalaby *et al,* 2009).

The potential of using sentinel -2 multispectral instruments was applied by Cardoso-Fernandes *et al* (2018) to map Li in Fregeneda-Almendra Salamanca, Spain and Vila Nova de Foz Côa, Portugal. Several remote sensing techniques such as band ratio, principal component analysis were applied. The occurrence of iron oxide and clay mineral were predicted in the study area. Non altered and hydrothermally altered zones were also discriminated in the study area. Li bearing pegmatite was also mapped in the study area using supervised classification approach. The supervised classification method used the land cover spectral signature and performed both PCA and maximum likelihood algorithms. Considering the results given in this work, Cardoso-Fernandes *et al* (2019) presented two new different approaches: (i) identification of hydrothermal alteration minerals associated with the Li-bearing pegmatite; and (cloud-free products, namely, Landsat-5 Thematic Mapper (TM), Landsat-8 Operational Land Imager (OLI) and Thermal Infrared Sensor (TIRS), ASTER, and Sentinel-2 MSI. The alteration mapping results differ from one image processing method to another Cardoso-Fernandes *et al* (2019). Supervised classification and principal component analysis were deployed in the Kalahari Desert in Namibia, in mapping the lithological units. The use of the ASTER data provided crucial information on the boundaries of the lithological units (Gomez *et al.,* 2005, Singh and Harrison, 1985).

ASTER and Phased Array L-band Synthetic Aperture Radar (PALSAR) data have been used for mapping lithology and gold-related alteration zones in the Um Rus area, Central Eastern Desert of Egypt (Amer et al., 2012). Principal component analysis and band rationing were applied on VNIR + SWIR bands of ASTER to discriminate lithological units. Spectral Angle Mapper (SAM) and Spectral Information Divergence (SID) classification methods were used to detect alteration minerals consisting of silicate, calcite and clay minerals associated with mineralized

granodiorite. Their field verification work indicated that the image processing methods were capable in lithological and alteration mineral mapping.

Principal Component Analysis (PCA), Minimum Noise Fraction (MNF - Green et al., (1988) techniques have been applied to VNIR + SWIR ASTER data for lithological mapping in Muslim Bagh ophiolite complex, Pakistan. The PCA discriminated metamorphic sole, sheeted dike complex, basalt and cherts, diabase dikes and gabbro bodies. The MNF transformed data detected sedimentary units, metamorphic sole, laterite, depleted harzburgite and diabase dikes/sills (Khan et al., 2007).

ASTER and Landsat data were used to map mineralized zones, whereby, Portable Infrared Minerals Analyzer (PIMA) was used, in measuring the spectral response of various rocks (Berhe, 2005). The digital number were of the lithological units were used in image analysis. The principal component analysis was used to study the tectonic structure of the study area and the application of band ratio for lithological discrimination of different rocks. Landsat data was found to provide more information on the lithological remote sensing as compared to ASTER as Landsat is more effective when used during the dry season. ASTER data was useful in providing structural and terrain features that assist in geological mapping.

The lithological mapping of gold in south Chocolate Mountains area, California, U.S.A were mapped by the use ASTER data (Zhang *et al*,.2007). In this study, various methods were used in extracting the information about the minerals. The maps derived from remote sensing methods were compared with maps derived from field work. He used principal component analysis together with maximum likelihood classification method, band ratio, and sub-pixel unmixing algorithms to detect significant alteration minerals. The use of the data was able to map the rocks which host gold minerals in the study area.

Mapping of ophiolitic rocks in central eastern desert of Egypt (Amer et al., 2010) was done by the use of ASTER band ratio techniques. The ratios used included $(2+4)/3$, $(5+7)/6$ and $(7+9)/8$. The principal component analysis was then applied to discriminate the ophiolitic rocks and grey granite and pink granite. The field work data verified the accuracy of the result achieved.

The band ratio, principal component analysis were used to map Gypsum outcrops using ASTER imagery in Tuzgolu basin, south Ankara, Turkey (Oztan and Suzen 2011). The techniques used were able to map evaporates and defined sulfate index using the thermal bands of ASTER. The results of the methods have been proven in the field and through laboratory analysis (X-ray diffraction (XRD) and Analytical Spectral Devices (ASD)).

2.3.3 Spectral Angle Mapper and Maximum Likelihood Classification applications

This mapping technique involve the comparison of the image spectra with reference one and finding their similarity by the calculation of the angular distance between them. On the other hand, maximum likelihood classification is a mapping technique which determines the probability that a given pixel belong to a certain class. It is calculated based on the spectral distance of pixels which are close together.

ASTER data was used in Alto Ligonha province Mozambique by Gemusse et al (2018) to map alteration minerals associated with Li bearing pegmatite. The satellite data was used to produce land cover maps using the spectral angle mapper classification technique. The technique was able to identify the spectral signatures of hydrothermal alteration of clay minerals (kaolin occurrences) which are associated with pegmatite Gemusse et al (2018).

In the region of Alto Ligonha region, different satellite products (namely ASTER, Landsat-8, and Sentinel-2) and different remote sensing algorithms were compared to target Li pegmatite Gemusse et al (2019) The algorithms include three supervised classification methods—minimum distance, SAM, and ML and one unsupervised algorithm: k-means clustering. The land cover classifications maps were compared as well as the performance accuracy of each classifier. Contrary to expected, the minimum distance attained the best accuracy while ML showed the worst performance Gemusse et al (2019) Perhaps these results reflect the quality of the training data. Despite the disparity between the results obtained with the different classifiers, Gemusse et al (2019) stated that the classification maps show clay minerals, such as kaolinite and montmorillonite, resultant from pegmatite alteration. These maps were validated through field investigations, geological maps and previous works and reports Gemusse et al (2019). The authors also noted that the satellite product that achieves the best accuracy for the SAM and minimum distance algorithm was the Sentinel-2.

Multispectral data were used to map banded magnetite in Nadu coast in Indian Peninsula (Chandrasekhar*et al*, .2001). In this study, various techniques were used in identifying the end members and the results compared with the spectral library obtained from the United States Geological Survey (USGS) spectral library. The spectral technique was then used to map the end members. The results were validated by the ground survey methods and it was found out that it was in agreement with the obtained remote sensing one.

ASTER data was used by Perrotta et al. (2005) to map Li bearing pegmatite in Vale do Jequitinhonha region, Brazil. In the study, the signatures of Li pegmatite were evaluated using the visible, near-infrared (VNIR), and SWIR data. The spectral angle mapper classification technique was then used to classify the ASTER image in collaboration with the mixture-tuned matched filtering (MTMF), having the last supervised method outperform the first since SAM was also sensible to roads, agricultural fields, or areas around the main drainage lines.

Lithological mapping of ultramafic complex in the Mordor Pound, NT, Australia (Rowan et al., 2005) was done by the use ASTER band ratios and relative absorption band depth (RBD), Matched Filtering (MF) and Spectral Angle Mapper (SAM) methods. In the study, mafic ultramafic rocks, alluvial-colluvial deposits were discriminated and classified based on the absorption features of Al-OH and ferric-iron. Granitoids rocks were mapped by the use of ASTER data. The data was processed by the use of false color composite technique and band ratio technique. The supervised methods which involved the use of maximum likelihood classification and spectral angle mapper were then used to discriminate the rocks (Massironi *et al.,* 2008).

In Eastern Anti-Atlas, Morocco, the use ASTER data has been utilized in mapping granitoids in the Saghro massif region. Remote sensing techniques such as false color composites (FCC), band ratios and principal component analysis (PCA) were employed to VNIR/SWIR and TIR data for detecting major lithological contacts and mineralized faults. The supervised maximum-likelihood (MLL) classifications and spectral angle mapper (SAM) were carried out on VNIR + SWIR data for discriminating granitoids rocks (Massironi et al., 2008).

Band ratios, certain color band combinations and the Spectral Angle Mapper (SAM) method have been used for mapping hydrothermal alteration minerals associated with Infiernillo porphyry copper deposit using ASTER data covering the San Rafale Massif, southern Mendoza

Province, Argentina (Di Tommaso and Rubinstein 2007). The hydrothermal alteration anomalies for predicting Cu-Au mineral resources have been delineated using ASTER data covering Oyu Tolgoi, Mongolia (Yujun et al., 2007). Gold-related lithologic and alteration minerals have been detected using ASTER data in the south Chocolate Mountains area, California, USA (Zhang et al., 2007).

2.4   Mineral exploration and radioactivity studies in Kenya

There are wide ranges of minerals in Kenya ranging from soda ash in Lake Magadi to fluorspar in kerio valley. Other minerals include the gold in certain parts of western Kenya as well as in lamu. These deposits occur either as oxides (magnetite, hematite, martite, goethite and limonite); carbonates (siderite and ankerite) or sulphides (pyrite and Pyrrhotite).

The activities due to quarrying and mining in Kenya account to less than one percent of the gross domestic product (GDP) with the majority of the contribution coming from the soda ash minerals (https://www.azomining.com/Article).

Ochieng (1993) described large bodies of titanium-vanadium-magnetite bearing layered norite-gabbro suite to the S.E. of Mt. Kenya in Marimanti area. He analyzed the ilmenomagnetite and found it to contain between 31.2 and 58.61% Iron oxide (Fe_2O_3), 14.2 to 35.16% titanium dioxide (TiO_2) and 0.84 to 0.88% Vanadium oxides.

The Bukura and Mbesa massive sulphides described by Ichang'i (1983) are examples of hydrothermal deposits. Ichang'i observed that, the ore consisted of pyrite, pyrrhotite, chalcopyrite and sphalerite. He suggested that hydrothermal fluids associated with the adjacent Mumias Granite were responsible for the mineralization.

Huddleston (1954) described the Bukura massive sulphide, as extending to an area more than one and a half kilometres. He estimated that the ore reserve was about 17 million tones down to a depth of 90 meters but suggested that it may exceed this figure, since lateral extensions are known to exist.

The coastal parts of Kenya have sedimentary iron-manganese deposits especially in the Kilifi area. Schissel and Aro (1992), referred to the Wilson cycle plate subduction of the early Proterozoic and the amalgamation of a Proterozoic supercontinent from 2000 to 1800 Ma to

propose a tectonic setting of the large sedimentary basins, which host large resources of iron and manganese in the very large Superior-type banded iron-formations. They deduced that this tectonic setting is consistent with the favored geological model in which huge iron and manganese deposits form. These deposits form on shallow continental margin shelves. Their continuous lateral bands also support a stable tectonic setting. Thoeliites within-plates may occur at continental margins near spreading centres (Nyamai *et al.,* 2003). Pohl and Horkel (1980) suggested that the magnetite deposit in Kurase group is a metamorphosed submarine exhalative mineralization associated with basic volcanics. Hydrothermal fluids have formed mineral deposits in this group.

There have been surveys conducted in Mrima hill to monitor the levels of radioactivity. High radiation levels were reported by Mangala (1987) in Mrima hill about 30km south of Kwale town. He attributed the levels to be due to thorium and uranium occurrence in the area. Titanium was also reported as one of the major constituents in rocks samples from Mrima Hill; the concentrations levels were observed to be in the range of 1- 9% with a mean value of 4.7% for most samples analyzed.

The Radiation Protection Board (RPB, 1999) reported high radioactivity patterns in the south Coast area due to the high radiation from Mrima hill. The report confirmed the results by Patel (Patel, 1991b). The Board carried out external radiation measurements at Mrima hill and also along the roads that were graveled using radioactive materials from Mrima hill. Surveying was also conducted in places such as Mombasa islands for the purpose of comparison. The radiation levels in this place was found to be low approximately 90 Bq/kg of Th-232 as compared to other places such as Likoni areas on the LungaLunga highway, the stretch from Msambweni to Kenya - Tanzania border point, where along this stretch, an average activity of 600 Bq/kg of Th-232 was recorded on the tarmac 15 mm deep, and as high as 1200 Bq/kg (Th-232) at the base gravel, 500 cm deep.

2.5   Summary of Literature Review in this study

The studies reviewed various remote sensing techniques used in geological mineral mapping; band ratio, color composite, the use of principal component analysis, the use of classified method

in mapping such as SAM and maximum likelihood. Some of the minerals identified using the above techniques include iron oxide in Tanintharyi coastal area in southern Myanmar. The study used, ASTER and Landsat data were used and the minerals were identified by the use of colour composite technique. Copper mineralization was mapped in Cuprite district in Nevada by the use matched filtering technique. The study used ASTER data and the results indicated hydrothermal alteration mineral zones. Iron deposits were identified by the use band ratio using ASTER and Landsat data in Wadi Bidah district, Saudi Arabia. The study results indicated the presence of sulphide deposits and zones of hydrothermal alteration.

Granite rocks were found to be a source of uranium by the use principal component analysis in Northern Iraq by the use of satellite infrared sensor data. Maximum likelihood classification technique was used in identifying Gabbro, carbonate, granite and mafic rocks in Allaqi-Heiani Suture in southern Egypt. The use of spectral angle mapper technique identified granitoids rocks for mineralized zones in Saghro Massif, eastern Morocco. Felsic rocks were mapped by the use band ratio techniques in Broken Hill, Australia, using ASTER very near infrared and shortwave infrared bands.

In general, mapping of minerals using remote sensing techniques require more spectral bands and smaller bandwidth. This is because, the information about minerals and rocks are found in the middle or shortwave and to some extent, the thermal region of the electromagnetic spectrum. Recent satellite launches, for example Landsat 8 have more bands as compared to earlier satellites, thereby enabling more information about minerals and rocks formations on the earth's surface.

Mapping of minerals at local scale, indicate the occurrence of minerals such as; pyrite, chalcopyrite limestone in Kenya. Titanium/magnetite has been mapped in S.E of Mt Kenya.

The sulphides ore has been observed to contain pyrite, pyrrhotite and sphalerite deposits in Bukura. The iron- manganese deposits have been identified in Kilifi area, in the coastal part of Kenya. This is attributed to the occurrence of early Proterozoic and amalgamation of Proterozoic supercontinent from 2000 to 1800 Ma to propose a tectonic setting of the large sedimentary basin which host large resources of iron and manganese.

The high radiation levels at Mrima hill have been attributed to thorium and uranium occurrence in the area. Titanium was also reported as one of the major constituents of the rock samples in Mrima hill.

In general, most mineral exploration activities in Kenya, has been done mainly through field work. The mineral exploration through thick weathered environment is usually a challenging task. The use of remote sensing techniques has been proved to be effective techniques in mapping minerals in other parts of the world, in areas not accessible. Applications of geological remote sensing and GIS for radioactive mineral mapping are not fully integrated into the activities of the Geological Survey of Kenya. This research aimed at the application of remote sensing to map radioactive minerals in Mrima hill Kwale County. There are possibilities that the area contains so many unexplored minerals.

Chapter Three: Theoretical Principles of Remote Sensing Techniques

3.1   Natural Radioactive Minerals and occurrence

Radioactive minerals contain radioactive nuclide in uranium, thorium and potassium (Sabins, 1997). The level of radioactivity of these minerals depends on concentration of natural radioactive nuclides. The emission of gamma, alpha and beta particles from unstable isotopes cause the radioactivity of these minerals.

Some of the minerals bearing uranium and thorium include; autunite, bassetite, carnotite, monazite, among others. In general, radioactive minerals are classified into two groups; syngeneic or epigenetic (Lambert, 1994). Syngenetic are minerals in which the minerals ore, are part of the rock, while epigenetic are minerals, in which they are formed by the addition of radioactive minerals to the host rock.

In granite rocks, the natural radioactive elements are found in the fine volcanic particles. They contain the highest concentration of radioactive minerals. The pegmatite rocks are one type in which these minerals occur. These rocks normally contain the rare earth minerals in addition, such as monazite that host uranium and thorium. It is also in pegmatite where uranium and thorium minerals such as uraninite and thorianite form. The rocks such as conglomerate and sandstone are due to weathering, erosion or deposition from sedimentary. These rocks normally have a high concentration of radioactive elements (Wilde*et al* 2013). Most of the uranium mines are normally in sandstone or conglomerate. Apatite hosts both uranium and thorium in its structure. The hydrocarbons in coal sometimes host these radioactive minerals. Coal and phosphate sometimes may contain enough uranium to be considered low grade uranium ore deposits.

3.2   Interaction of electromagnetic radiation for minerals and rocks identification

Rocks are assemblages of minerals and in turn, comprise different molecules and elements. The components of rocks and minerals include; silicon, aluminum, iron, calcium, sodium, among many others. The spectra signature of minerals is dominated by the effects of less- common ions and the molecular structures in which they are bonded (Drury, 1993). The different types of rocks and minerals have different spectral signatures thus different curves. These form the basis under which they are identified using remote sensing techniques.

3.2.1   Spectral characteristics of minerals

The absorption features in the reflectance spectra data are caused by two major types of interactions between photons and crystal lattices of minerals, called electronic transition and vibrational processes. The electronic transition includes crystal field effects and charge- transfer while the vibrational processes embrace overtones and combination tones (Drury, 1993). Figure 3.1 shows the reflectance spectra curves of some iron-bearing minerals.
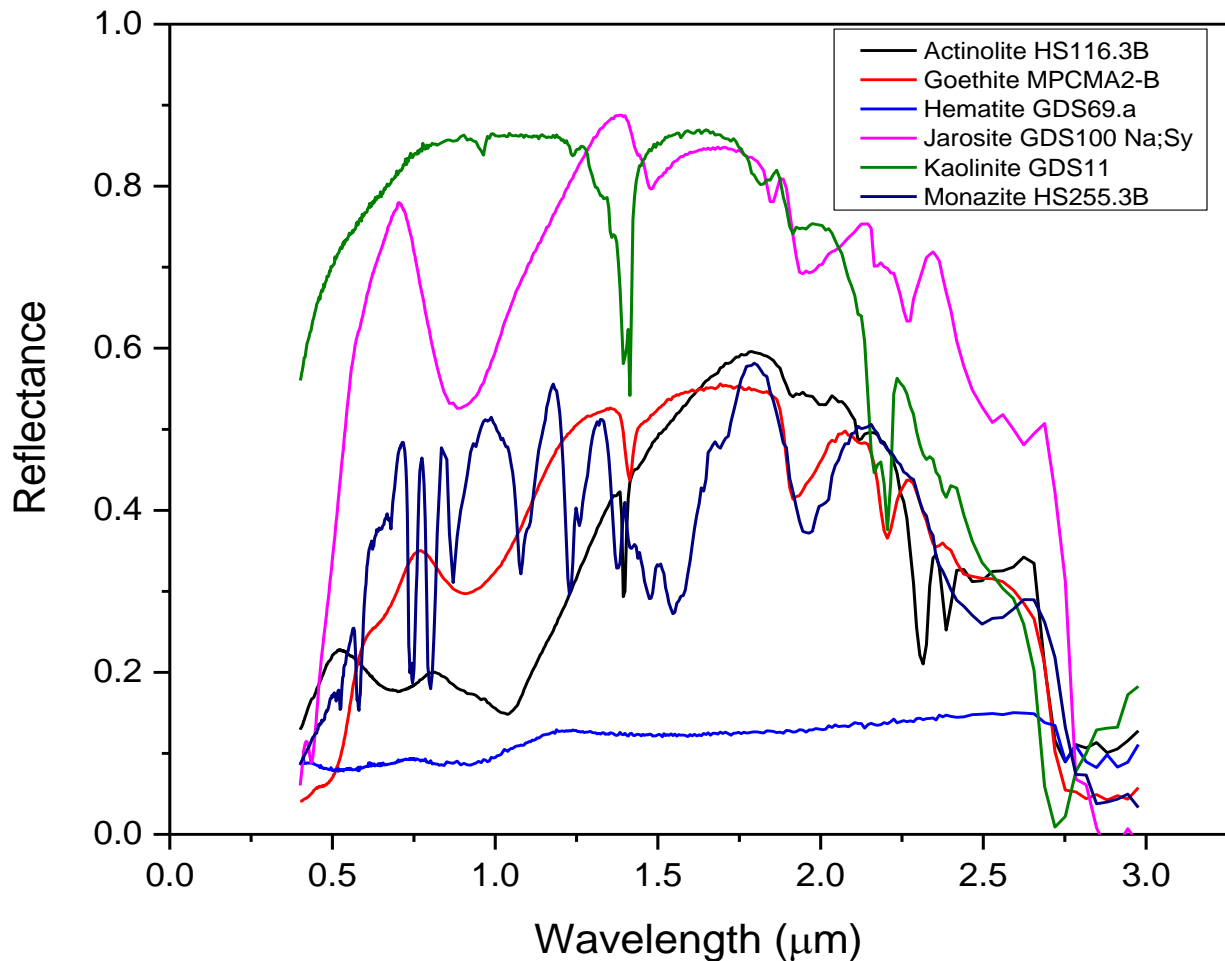
Figure 3.1: Spectra curves of clay and iron-bearing minerals (www.usgs.gov/speclib).

The absorption and reflection at various wavelength regions are represented by the troughs and peaks as shown in figure 3.1. These are caused by effects such as lattice distortion. The distortion is caused by effect of charge transfer and crystal field effect. These are normally common in minerals such as iron oxide bearing minerals. Minerals which have absorption at 1.9µm normally contain water but a spectrum that has a 1.4 µm but no 1.9 µm absorption indicates that only hydroxyl is present.

3.2.2   Spectral characteristics of rocks

Rock's spectral characteristics normally depend on the composite of their minerals. It also depends on other factors such as the environment, the content of water as well as surface condition. Different rocks have different spectra curves. Figure 3.2 shows the reflectance spectra of specific igneous rocks.
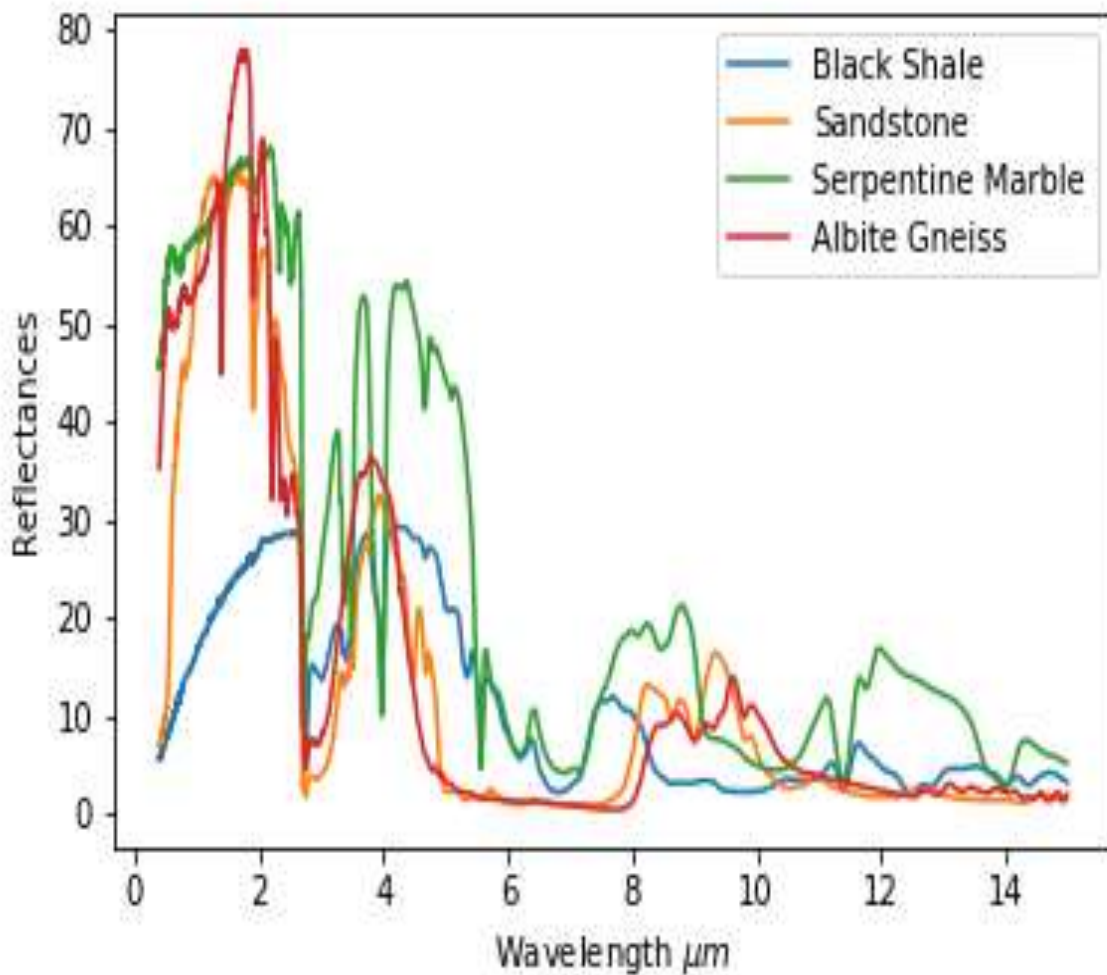
Figure 3.2: spectra curves of igneous rocks. (Source: JPL spectral library.)

Rocks which have low content of iron, Mg as well as significant content of silica show relatively high reflectance and they include rocks such as granite and felsic. They have high absorption in

the 0.9µm wavelength range due to iron content. The water content cause absorption in the wavelength ranges of 1.4, 1.9, 2.2 and 2.3 µm. Water, OH ⁻ carbon dioxide influences the spectral features of rocks such as the sedimentary rocks. For sandstone, the presence of fluid inclusions and calcareous cement, cause absorption bands at 1.4, 1.9, 2.2 and 2.3µm. (Lei, 1999). The plot of the spectral reflectance of vegetation associated with radioactive minerals is as shown in figure 3.3
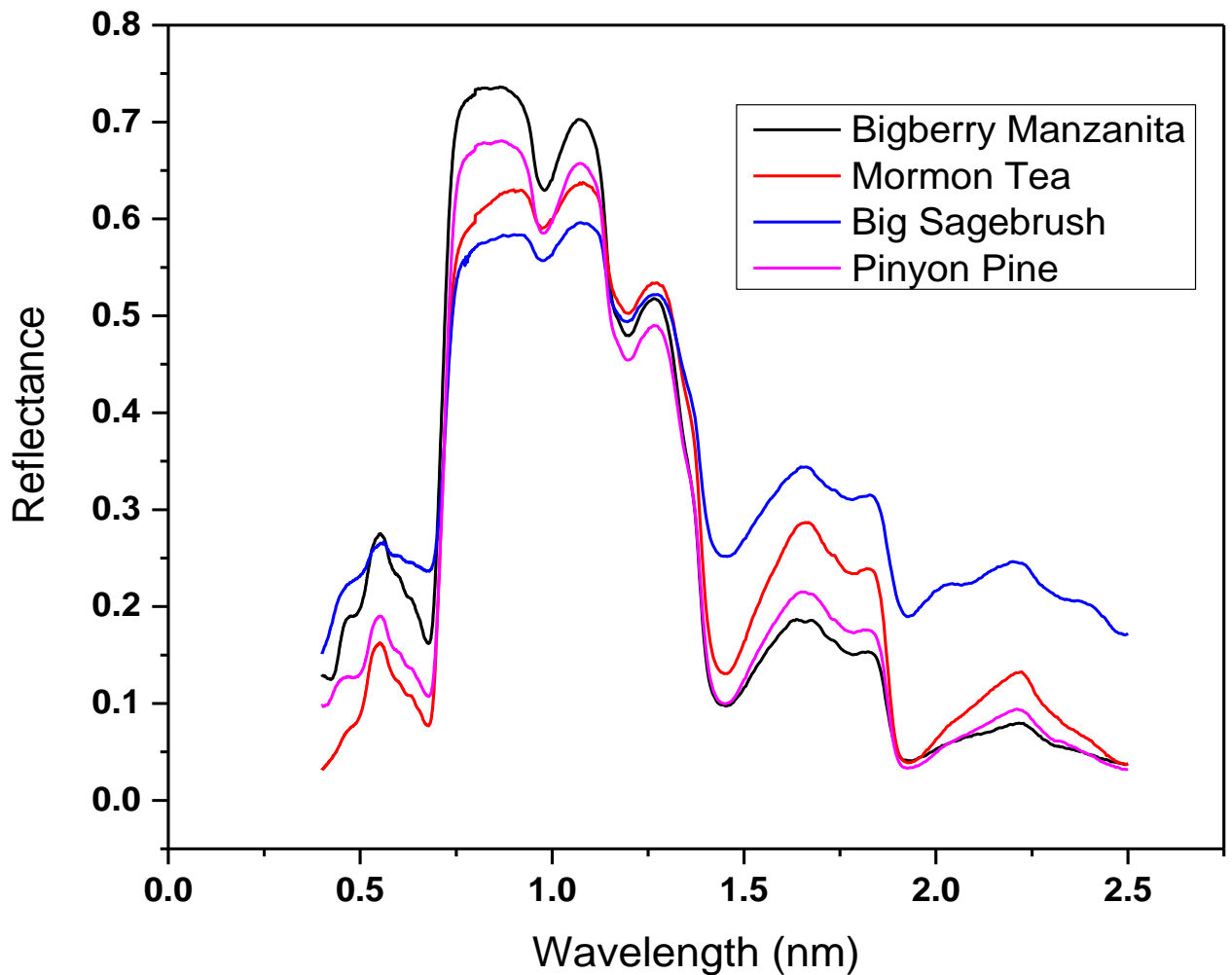
Figure 3.3: Reflectance spectra curves of vegetation associated with radioactive minerals. (Source: JPL spectral library).

3.3 Remote Sensing Minerals Mapping Techniques

The satellite download data contain errors related to the atmosphere, sensors or even the platform. Before carrying out spectral analysis of these data, these errors have to be corrected. The process of correcting out these errors before spectral analysis of the data is called preprocessing. The atmospheric errors can be corrected by a technique available in the ENVI 5.3 software called Fast Line-of-sight Atmospheric Analysis of Hypercube (FLAASH) using a standard equation given by:

$$L = \left(\frac{A_\rho}{1-\rho es} \right) + \left(\frac{B_{\rho e}}{1-\rho es} \right) + L\alpha \qquad\qquad 3.1$$

Where L =solar wavelength range, ρ =surface reflectance of the pixel, s = spherical albedo of the atmosphere ρe = surface reflectance average of the pixel and the surrounding environment, , $L\alpha$ = backscattered radiation by the atmosphere, A and B are coefficients which depend on atmospheric and geometric conditions.

By applying the above method available in ENVI software, the errors due to atmospheric can be corrected prior to spectral analysis. The errors due to the sensor can be corrected by applying the radiometric calibration module available in the ENVI software.

The techniques which have been applied remotely in mapping minerals include; principal component analysis, color composite, spectral angle mapper, band ratio and maximum likelihood The spectral dimensionality of the data may be achieved by applying the method known as the minimum noise fraction, which maps the majority of the material of interest in the pixels. Analysis of the end members can be done by other techniques, which include; spectral angle mapping and spectral unmixing. Spectral unmixing is important when a pixel contains many objects which result into different response for the pixel and therefore it's needed in breaking these materials into their distinct constituents and their relative proportion in a pixel.

3.3.1 Color composite

This technique uses the idea of combining the information in the multispectral datasets so that it can be visible. The human eye can be able to see the reflectance from the combination of the red, green and blue portion in the electromagnetic spectrum. The combination of band 3, 2, and 1 in the Landsat TM sensor are for the true color. Any combination displayed as RGB apart from the true color is called false color composite (Ahmed, *et al.,* 2014). This technique is the basis for other remote sensing techniques in image processing.

3.3.2 Band ratio

This is an image processing technique which involves one band divided by another one, based on the materials spectral characteristics in the study area. This result is the ratio of the spectral reflectance of one band to a spectral reflectance of another band. Materials on the surface of the earth which are similar can give different brightness values due to factors, such as; slope, seasonal changes, and illumination angle from the sun. This can influence the viewer to give out false interpretations. To minimize such factors which lead to false interpretation, band ratio is used because it minimizes the effects of these environmental conditions (Jensen and Lulla, 1987). The band ratio can also provide additional information which cannot be found in a single band display. This is helpful when discriminating between the soils and vegetation (Satterwhite *et al.,* 1984). In the study, the band ratios method to identify rocks types and minerals was employed (Gad and Kusky 2007).

3.3.3 Principal Component Analysis

Principal component analysis (PCA) is a linear transformation to reduce such information redundancy in multispectral images; which decorrelates multivariate input data by rotating and/or translating the axes of its original space, so that the data can be exemplified without correlation in a new space that should be capable to identify different features and surface types easier. Different bands of multispectral data are often correlated and thus contain similar information i.e. have similar visual appearances. This correlation means that there is redundancy of information. The principal components (PC) transformation is used, to reduce this data redundancy, by compressing multispectral data sets and calculating a new coordinate system

(Sabins, 1999). The application of the PC on the present data is to compress all of the information contained in an original n-channel (band) data set, into fewer number of channels or components, that could be displayed separately as single stretched PC-images, or as component in color composite PC-image (Vincent, 1997).

The equation 3.1 is used in projecting the n spectral bands into final n principal components:

$$\rho_k = \sum_{i=1}^{n} a_{ik} DN(i)$$

3.2

Where:

ρ_k is the kth principal component value for a given pixel, $DN(i)$ is the digital number of the ith spectral band for a given pixel and a_{ik} give the projection coefficients calculated by the principal component algorithm for projecting digital numbers from the n spectral bands onto the n principal component vectors.

The data from the above equation is then translated into a new origin along the major axis. The variances obtained from the principal components are called eigenvalues (E. Chuvieco*et al..*, 2010). The remaining variance decreases as the principal component increases. The variances add up to 100% of all the principal components, but it's only the first three components which provide most of the information.

3.3.4   Crosta technique

This is the method whereby the spectral bands are reduced in the input of principal component; therefore, making sure that some materials are not mapped out thereby increasing the chances of mapping the materials of interest. The method is effective when the knowledge of the materials to be mapped is well known. Raw data is used while performing these techniques without any corrections such as radiometric corrections.

The eigenvector signs and magnitude, provides the spectral information of rocks, soils mapped into each principal component.

3.3.5   Spectral unmixing

Spectral unmixing is the procedure by which the measured spectrum of a mixed pixel is decomposed into a collection of constituent spectra, or endmember, and a set of corresponding fractions, or abundances, that indicate the proportion of each endmember present in the pixel. Endmember normally correspond to familiar macroscopic objects in the scene, such as water, soil, metal, vegetation, etc. This involves the use of the module available in the ENVI software known as Spectral Hourglass scheme (Kruse et al., 2003). The method is used to reduce the data in terms of the dimensionality. It is done by starting with the minimum noise fraction method and then followed by the use of the index purity mapping technique in order to determine the purest pixel in the image. A tool in the ENVI software known as n-Dimensional-Visualizer tool (n-D-Vis) is then used to extract the end member. The final step involves comparing the end member with those from the USGS spectral libraries and then the application of spectral angle mapper technique (Kruse *et al.,* 1993). The method is applied when dealing with hyperspectral data sets and may not be useful when it comes to multispectral datasets.

3.3.6   Supervised classification

This is a method which is used to get the information from images obtained from remote sensing datasets. It involves sufficient knowledge of known pixel. This process of generating parameters to be used is called training.

Training sites involve areas which represent known land cover category that appear uniformly in the image. The mean and variances for each are calculated from all the pixels in the study area. They do have steps of operations which must be followed when carrying out this method of classification. The steps include Training sites definition; Signatures extraction, and Image classification.

These training sites are worked on by digitized features. More training sites produce better results and this increases the accuracy of the image classified and also the interpretation of the results. More training sites are normally selected. The statistical characterization of the information is normally created after the training site areas have been digitized. The most commonly used supervised classification methods are discussed in the subsections below.

3.3.6.1   Maximum likelihood

This is the technique used to classify image which involves the calculation that a given pixel belongs to a particular class using probability. It is calculated on the basis that the spectral distance of pixels, which are close together. These pixels are classified together based on the statistical distribution. The probability threshold must be specified in order for the pixels to be classified to a particular class less all pixels will be classified. The pixels with the highest probability will then be assigned to a particular class. The geological mapping has been effectively mapped using this method (Gomez, 2005; Massironi, 2008). Maximum Likelihood Classification (MLC) assumes a multivariate normal distribution for the individual class signatures.

3.3.6.2 Spectral angle mapper

This is the method of classification whereby the angles between the image pixel and the region of interest data are compared. The calculation of the angular distance between the end member and the image determines their similarity. Those pixels which are similar are classified together as one class (Yuhas et al, 1992; Kruse *et al,* 1993). The smallest angle between the pixels indicates very close resemblance to the reference spectra. The equation describing the process is shown in equation 3.3:

$$\alpha = cos^{-1}\left[\frac{\sum_{i=1}^{nb} t_i r_i}{\sqrt{\sum_{i=1}^{nb} t^2}\sqrt{\sum_{i=1}^{nb} r^2}}\right] \qquad\qquad 3.3$$

Where: nb the number of bands in the image, t pixel spectrum, r reference spectrum and α spectral angle.

Chapter Four: Materials and Methods

4.1   Introduction

The chapter describes the study area, the remote sensing data and software used, various remote sensing techniques used in mapping types of rocks in the study, and the data validation process applied.

4.2   Study area Description

The case study lies on the coastal part of Kenya located at 4° 29'l0"S; 39° 15 '10'' E coordinate south in Msambweni constituency, Kwale County. It is approximately at a distance of 80km south-west of the port city of Mombasa. It forms a small elliptical hill that rises some 750 feet above the coastal plain. The area forms a Centre for alkaline igneous complex and it is covered by ferruginous residual deposits, which are as a result of much weathering. The area lies south of the equator and its climate is influenced by the monsoon winds. The amount of rainfall received in the area annually ranges from 965mm to 1270mm. The area receives two rainfall patterns which include two long and Shorty rainy seasons. This is attributed to the monsoon winds experienced in the area.

The study area is characterized by high temperatures with an annual average of 27.9^0 C. The month of February is the hottest month while July is the coolest month with an average temperature of 22.70C. The area is covered majorly by *Dovyalis keniensis* E. V.genus which contains 18 species (Sleumer,1975). Some of the species include the Asparagus sp which contains vegetation such as Mormon tea, sagebrush and pynon pine, which are all associated with radioactive mineralization (Gillman, 1949). The area is characterized by a number of rock formations such as sedimentary, alkaline, Duruma sandstone and igneous series. It is rich in Fe, Mn, and rare earth metals which are associated with U and Th bearing minerals namely monazite (Horkel et al, 1984, Mangala, 1987).

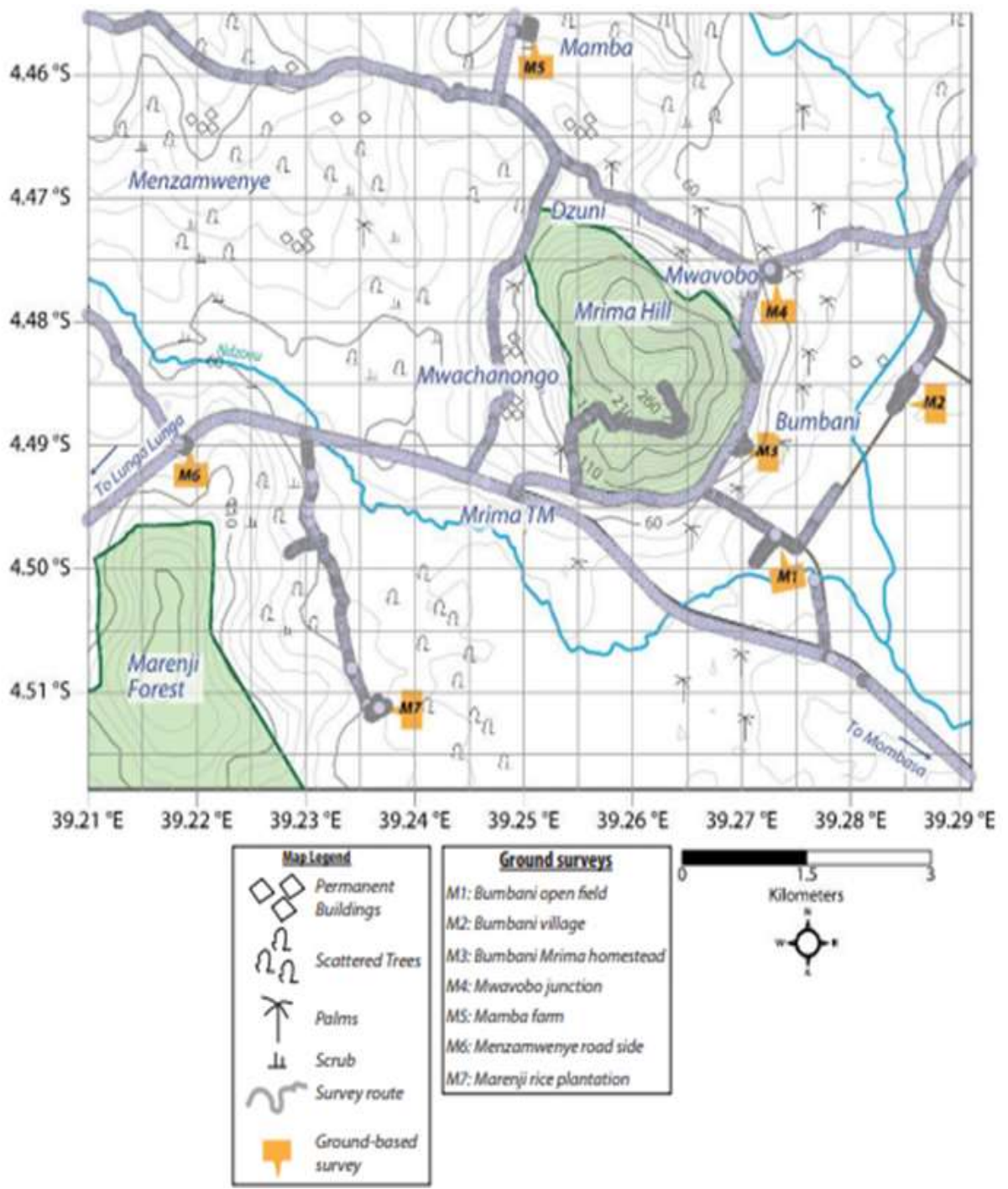Figure 4.1 and 4.2 shows the location and geology of the area of study (Kaniu & Angeyo, 2018).

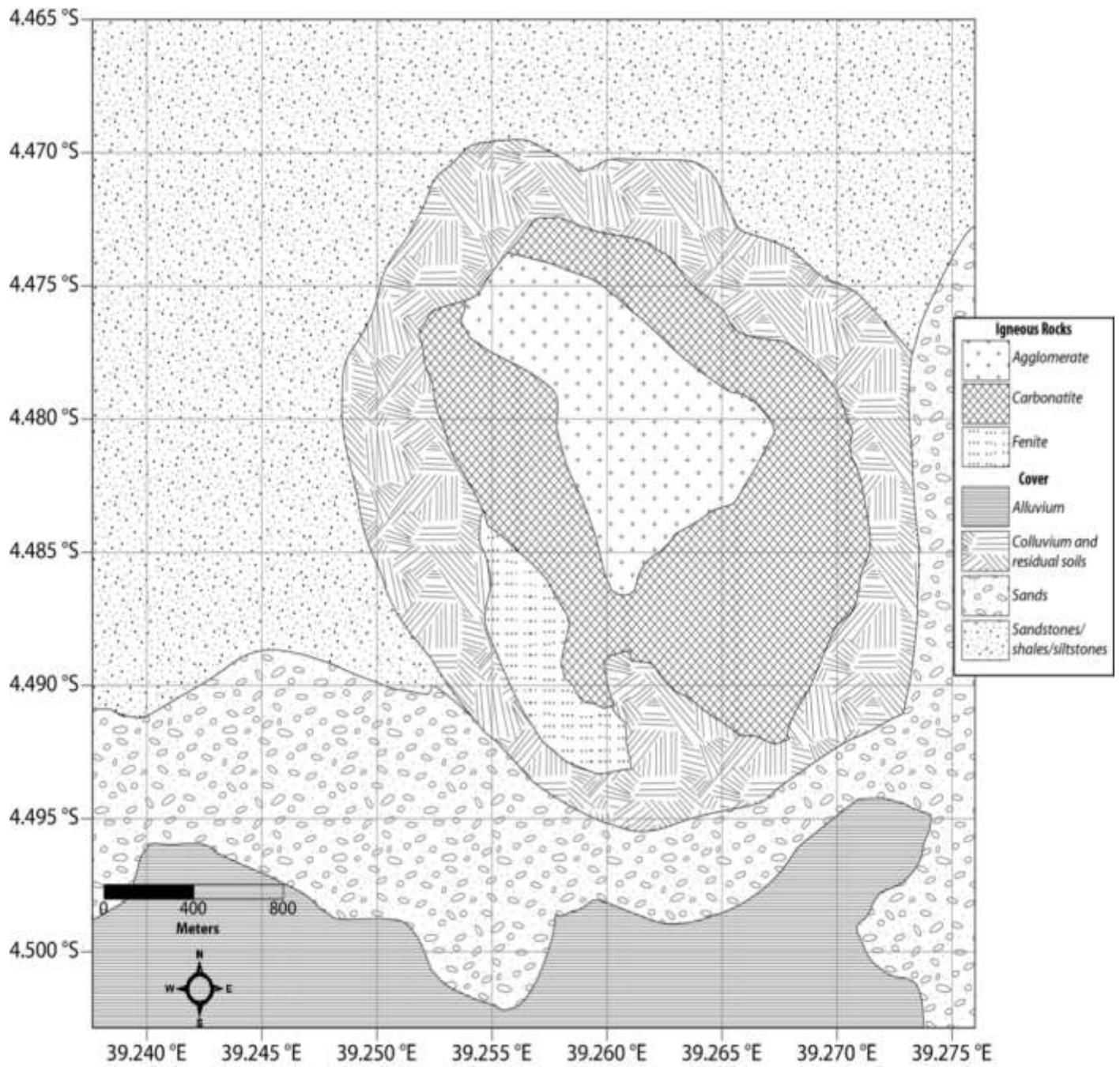**Figure 4.1: A map of Mrima hill in Kwale county showing the area of study(Kaniu, 2018)**

Figure 4.2: Geology of Mrima hill Kwale County from (Kaniu, 2018)

4.3   Satellite data and software

Landsat 8 acquired on 30th March 2016 was used in this study. The orthorectified scenes were acquired from the NASA's Earth Explorer web portal (http://earthexplorer.usgs.gov/).

In principle, Landsat 8 data image consist of OLI sensor and TIRS that has a total of eleven (11) bands; seven (7) in the visible and near infrared, two (2) in the thermal infrared region, one (1) panchromatic channel and one (1) cirrus channel. The spatial resolution is 30m for visible bands, 15m for panchromatic band and 100m for the thermal bands. Landsat 8 images, approximately 952-962 megabytes, were obtained in file format (TIFF) on diverse dates between 15th January and 30th March, 2016. The Landsat data file has data in radiance format, but was later converted to reflectance format, the appropriate format, where materials on the surface of the earth interact with the electromagnetic radiation is recorded by the sensor onboard Landsat 8 satellite. Total of six (6) Landsat 8 images data were downloaded, but only one, which was collected on 30th March, 2016 was used in this study, because it had the minimum cloud cover, minimum noises and artifacts.

Table 3.1.Shows the description of the study location, in terms of the paths and rows, which are specific of the area and the corresponding coordinates, and when accessed. To retrieve the spectral responses of materials on the surface of the earth, the satellite image capture dates were carefully chosen to correspond to the period when the cloud cover was low and the vegetation density was minimum during the dry season. Mrima hill is sub-tropical region and has dense vegetation and receives high rainfall, characterized by two distinct long and short rainy seasons.

Table 4.1. Path and row coordinates and the dates of the Landsat OLI scenes used

Location	Path	Raw	coordinates	Date (day/month/year)
Mrima hill	166	63	4° 29'lO"S; 39° 15 '10'' E	30/03/2016

ENVI software version 5.3 and ArcGIS version 10.3 were used to extract spectral information of various materials on the earth's surface, such as; lithology, hydrothermal alteration, and structure, through digital image processing; preprocessing, image enhancement, and classification of remote sensing data. The software was purchased from ESRI, a local company which specializes in spatial satellite software and products.

4.4   Remote sensing data processing techniques

Figure 4.1 shows the sequential steps followed to extract the spectral information of materials of interest:

a) Removal of clouds by the application of the Preprocessing procedure.

b) Image enhancement for identification of rocks and minerals in the study area;

c) Performing maximum likelihood classification (MLC) method –for identification of rocks and vegetation associated with radioactive minerals in the study area, and

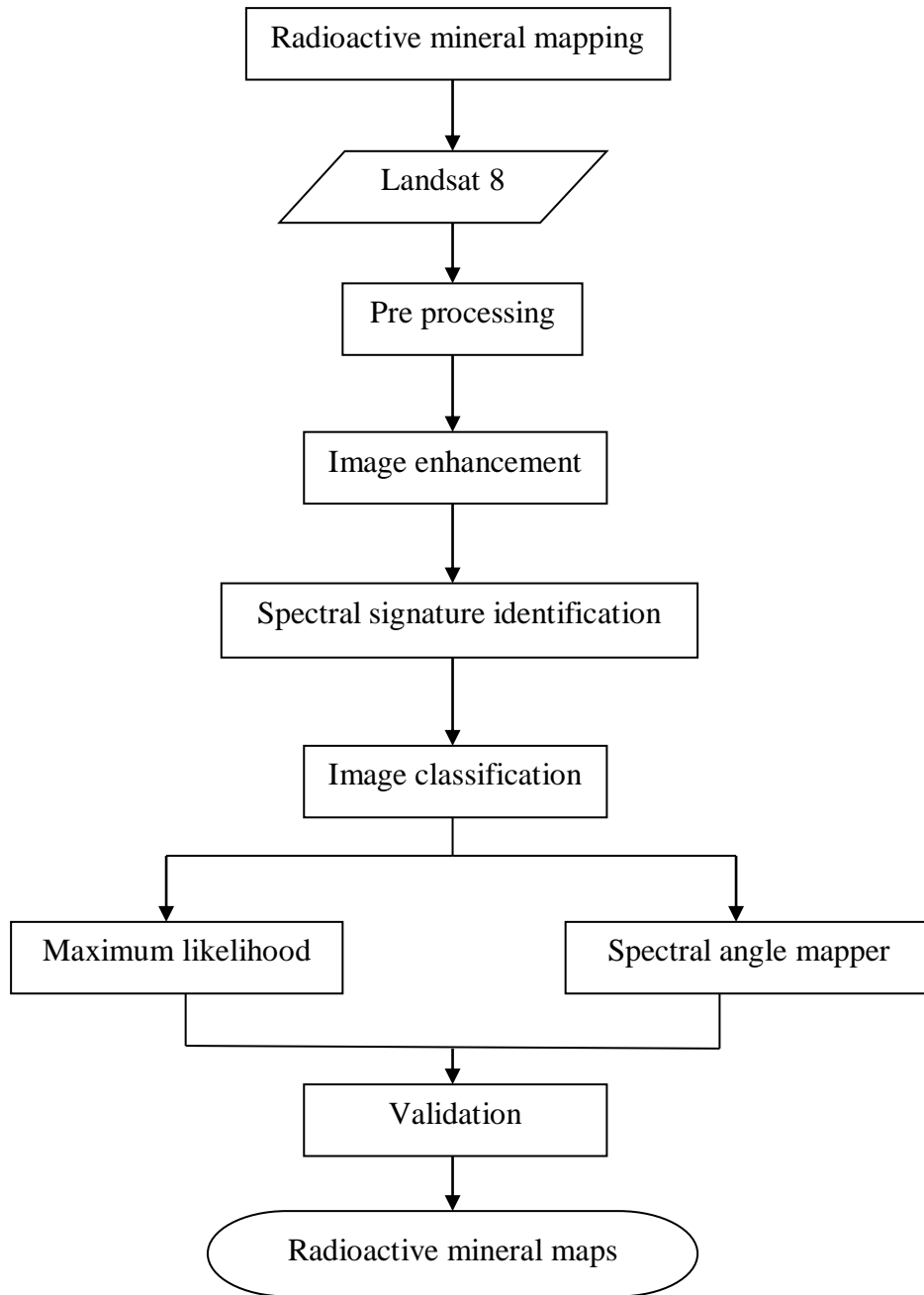d) Validation of the results using existing; radiometric and geological data of the study area.

```
                    ┌─────────────────────────────────┐
                    │  Radioactive mineral mapping    │
                    └─────────────────────────────────┘
                                    │
                                    ▼
                    ╱─────────────────────────╱
                   ╱      Landsat 8          ╱
                  ╱─────────────────────────╱
                                    │
                                    ▼
                    ┌─────────────────────────┐
                    │     Pre processing      │
                    └─────────────────────────┘
                                    │
                                    ▼
                    ┌─────────────────────────┐
                    │   Image enhancement     │
                    └─────────────────────────┘
                                    │
                                    ▼
                ┌─────────────────────────────────┐
                │ Spectral signature identification│
                └─────────────────────────────────┘
                                    │
                                    ▼
                    ┌─────────────────────────┐
                    │   Image classification  │
                    └─────────────────────────┘
```

Figure4. 2. Steps and coupled methodology for radioactive minerals retrieval.

Figure4. 2. Steps and coupled methodology for radioactive minerals retrieval.

4.4.1 Landsat data preprocessing

The Landsat 8 acquired on March, 2016which contain eleven (11) spectral bands were analyzed for surface earth information.

The acquired Landsat 8 images were first converted into an image (*.img*) file format. In general, prior to data analysis, these image data were corrected for errors related to the atmosphere, sensors or even the platform; mounting of the sensor in the satellite platform, view angle of the sensor, and other artifacts.

The atmospheric errors were corrected by a technique available in the ENVI 5.3 software, Fast Line-of-sight Atmospheric Analysis of Hypercube (FLAASH).The errors due to the sensor were corrected by applying the radiometric calibration module available in the ENVI software, whereby satellite data is converted into reflectance from the initial format in radiance, in addition, to characterize the various materials under study.

Cloud covers were found in the Thermal Infrared (TIR) region by first converting the digital number values to temperature brightness values using the ENVI software.

The dark parts were found to correspond to cloudy areas in this study. It was found to contain the lowest temperatures values. Based on this variation in temperatures, threshold was determined, less than 240K for this study, classified as the dark part, and then was masked out, but replaced by searching out an image which is cloud free in the same pixel. The dark pixels were replaced and then assigned new values based on the mean TIR band image. The temperature differences enabled to clearly distinguish between the cloudy and non- cloudy TIR bands in the study area. This was done using Matlab algorithm.

4.4.2 Vegetation analysis: Calculation of Normalized Difference Vegetation Index (NDVI)

The interpretation of multispectral images for geological information is impeded by vegetation cover especially in densely vegetated area. To get the geological information, it's important to remove vegetation component by suppressing them. For this study the forced invariance technique which is embedded in ENVI software to suppress the vegetation component was employed (Crippen and Blom, 2001).

The process involved approaching the following steps which included masking out barren or sparsely vegetated area by the use of Normalized Difference Vegetation Index, application of forced invariance technique in subtracting the spectral response of vegetation only in vegetated areas; and lastly the combination of the processed vegetated areas with the barren area.

In order to mask vegetation in Landsat 8 images, calculation of the vegetation index is done. The index applied includes the NDVI and was used to determine the threshold value to mask vegetation.

The NDVI is defined as;

$$NDVI = \frac{NIR - \mathrm{Re}\,d}{NIR + \mathrm{Re}\,d}$$ (4.1)

here NIR is the Digital Number value of Near-Infrared band, and *Red* is the DN value of the red band radiation. The threshold NDVI value used to mask vegetation in the study area was 0.25 which is the NDVI value range for shrubs and grasses in the study area.

4.4.3 Rocks and Minerals Identification in the Study Area: Band Ratios

This method of image processing technique involved division of one band by another band of the material of interest (Sabins, 1999). For examples rocks such as; alkali granite, sandstone, serpentine and carbonates which are all associated with radioactive minerals. The result is a spectral ratio one band to another band.

This method is used to identify certain materials such as minerals or rocks which cannot be observed by a single band. This method involves selecting a band with high reflectance for minerals or rocks as a numerator divided by the one with the lowest reflectance as the denominator. The bands are put as input in the ENVI module. The ENVI band ratio interface module has for input, has the option of eleven bands, each band is assigned a certain wavelength range in the electromagnetic spectrum for a single material identification. For example, band 4 has a wavelength range of between 0.64 - 0.67 µm, where iron oxide has high reflectance. The iron oxide was mapped by the use 4/2 ratio since it has high reflectance in band 4 while it also has high absorption in band 2. On the other hand, the ratio 6/7 was used in mapping clay

minerals because clay minerals have high reflectance in band 6 while also having high absorption in band 7.

The following ratios were used in discriminating the rocks and minerals of interest using Landsat 8 data; (6/7, 6/5, 4/2), (6/4, 4/2, 7/3 Cardoso-Fernandes *et al* (2018)

4.4.4 Rocks and Minerals Identification in the Study Area: False color composite

The combination of the three primary colors was applied to highlight the geological features in the area of study. The features included; the structural features, the vegetation cover, sedimentary and igneous rocks.

For lithological mapping, the following color combination were used ;(5, 6, 4), (7, 6, 5), (7, 6, 2). The bands were applied by individually inputting the 8-bit gray scale reflectance bands into the ENVI band combination interface module. The bands were selected based on the known mineral absorption and reflectance features.

4.4.5 Minerals Identification: Principal Component Analysis

The seven reflectance bands of Landsat 8 data were used to carry the procedure of principal component. This method was used in highlighting the minerals of interest in the case study. The first three principal components generated, accounted for more than 95 % of the variance in the original data Bands of multispectral data. The redundancy of data was reduced by applying this method on the multispectral data. The signs and loadings of the eigenvectors indicate the spectral information of minerals in the study area. In this study, the principal components were determined by the use of MATLAB algorithm for mineral identification (Appendix 1)

4.4.5.1 Minerals Identification: Crosta Techniques

This method is used whereby the spectral bands are reduced for the input of principal component, thereby increasing the chances of mapping the materials of interest. For clay minerals, band 2, band 5, band 6 and band7 were used while for iron oxide minerals, band 2, band 4, band 5 and band 6 were used. The signs and values of the eigenvector loadings which were generated by Matlab algorithm provide the spectral information; reflectance and absorption about these minerals (appendix 1).

4.5 Classifications of rocks and vegetation

The process of assigning pixels which are unknown to a particular class depending on their properties is known as image classification (Ahmed, *et al.,* 2014). Two major types of classification include; the supervised and unsupervised classification methods. In the unsupervised classification, the software analyses an image without the user providing sample classes, the user can specify the algorithm the software will use as well as the number of the output classes. In supervised classification, the user provides the training data and directs the software to use these training sites as references for the classification of all other pixels in the image.

4.5.1 Maximum likelihood classifier for rocks and vegetation classification

The rocks are classified into different classes based on the spectral distance of pixels which are closest. In the study area, the remote sensing data was classified using Region of Interest (ROI) of the spectral signatures of the rocks types available in the ENVI 5.3 software spectral library database for the following rocks; alkali granite, sandstone, serpentine, shale and carbonate rocks. For rocks identified, high probability threshold for each class was set at 0.7 for optimal input in the ENVI interface module. The probability values were determined by varying the input values for between 0.1 to 1.0, to obtain optimized output.

This method of image classification depends on determining the probability that a given pixel belongs to a certain class of material of interest in the study area.

The procedure was repeated for classification of vegetation associated with radioactive minerals. The vegetation plant species used in this study included; bigberry manzanita, sagebrush, Mormon tea and pynon pine.

4.5.2 Spectral angle mapper for rocks and vegetation classification

The Spectral Angle Mapper technique was applied whereby the angle between the spectra and reference was calculated. The principle for this image classification technique is that, the smaller the angle between the image spectra and the reference spectra, the closer the resemblance of the

materials of interest. Reference spectra available in spectral libraries and or from field observations were used in this study (Kruse et al., 1993).

The SAM classification enhances the target reflectance characteristics and also has the ability to discriminate different rock types. The reference spectra selected for training data include; alkali granite, basalt, sandstone, quartz monzonite, shale and marble rocks which were obtained from ENVI 5.3 software spectral library. A single value for maximum angle in radians was set for all classes by default, according to the rock types of the training data input.

4.6   Validation of the Remote Sensing Data of the Study Area

The results were validated by using existing radiometric data and geological map of the study area by overlaying with classified image of rocks and minerals of the study area using QGIS software. Overlay is a GIS operation that superimposes multiple data sets (representing different themes) together for the purpose of identifying relationships between them. An overlay creates a composite map by combining the geometry and attributes of the input data sets.

The software i.e. QGIS, is an open source which is used in viewing, editing and analyzing geospatial data. The user normally edits, analyze the spatial information as well as export graphical maps. The software support data in raster and vector layers.

Prior to overlaying of the data, the geological and radiometric maps of the study area were first georeferenced, so that all of them are in the same georeferencing system. We used the interpolated radiometric data of the study area for validation with the botanical indicators.

Chapter Five: Results and Discussion

5.1   Introduction

This chapter present results of the Landsat 8 data where several image processing techniques were used to delineate mineralization and rock types; iron oxide, clay, hydroxyl, ferrous, granite, sandstone, serpentine, and carbonates rocks and discusses the validation of the result.

5.2   Rocks and Minerals: Band Ratios results

Figure 5.1: shows the various types of minerals in the study area using the band ratio Landsat OLI ratio image (6/7, 4/2, 6/5 in RGB).

Figure 5.2: shows the different types of rocks in the area of study associated with radioactive minerals using the band ratio of Landsat OLI ratio image (6/4, 7/3, 4/2 in RGB).

The different types of rocks and minerals were processed and interpreted in the study area using the multispectral images of Landsat 8 data. For iron oxide minerals, bands 2 and 4 were used to identify them. The minerals in iron oxide include; jarosite, hematite and limonite minerals. These minerals show in band 4 to have high reflectance and band 2 having high absorption. On the other hand, the use bands 6 and band 7 identified clay and carbonate minerals. This is because they exhibit highest reflectance and absorption in band 6 and 7 respectively (Han et al., 2015). Altered rock were identified in the area by the use of 4 /2, 7/3, 6/4 ratios

In general, the band rationing enhances materials of interest on the surface of the earth which otherwise couldn't be seen by raw bands. It is therefore useful in hydrothermal mapping of alteration zones of minerals (Di Tommaso. 2007; Rockwell et al. 2008; Pour and Hashim. 2011). For example, iron oxide minerals in the area were identified by the use of 4/2 ratio because of the high reflectance of the mineral in the red region of the electromagnetic while it also has high absorption in the blue region. On the other hand, 6/7 ratio was used in mapping clay, kaolinite and montmorillonite minerals because of its reflection properties in band 6 and the high absorption in band 7 respectively. The ferrous minerals were identified using the ratio 6/5 because of their high reflectance in band 6 and very high absorption in band 5 (Gupta, 2003).
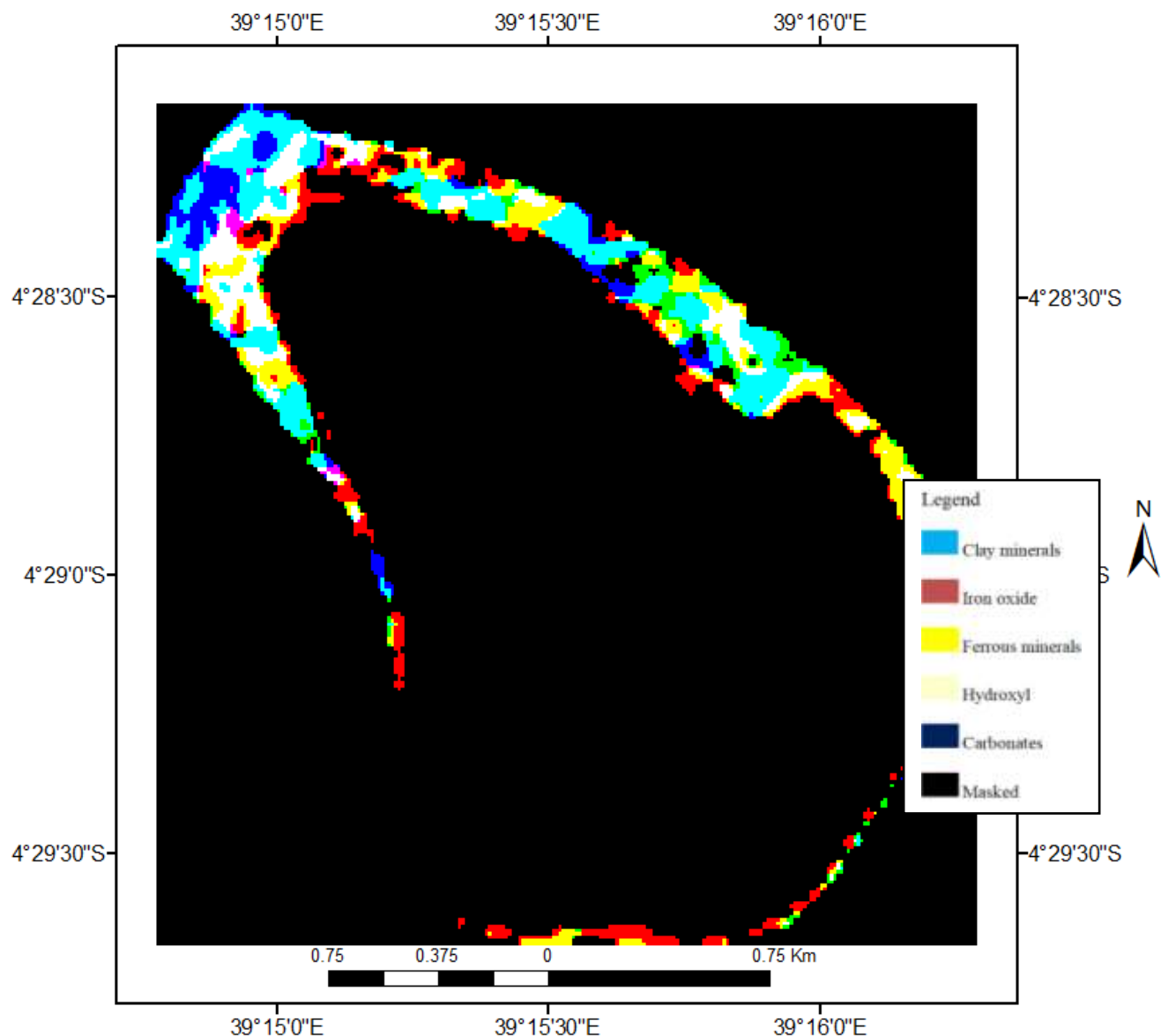
Figure 5.1: Landsat OLI ratio image (6/7, 4/2, 6/5 in RGB)

The ratio of 6/4, 7/3, 4/2 for Landsat 8 was used to highlight different rocks in the study area. This is because Serpentine rock exhibit high reflectance in band 6 due to the minerals contained in it while high absorption in band 4. Granite, on the other hand, has high spectral reflectance in band 7 and high absorption in band 3. Carbonates have high reflectance in band 4 with significantly high absorption in band 2. Therefore, the ratio 6/4 represents serpentine rocks while granite rocks are represented by the ratio 7/3 and carbonate rocks by 4/2. The color composite of these ratios shows serpentine rocks represented by the cyan pixels. Granite rocks are represented

44

by yellow pixels while the carbonates are represented by the magenta pixels as shown in figure 5.5.

The band rationing technique is important in highlighting the hydrothermal alteration of rocks. This is because they provide more information about certain features which cannot be seen by using the raw bands (Di Tommaso. 2007; Rockwell et al. 2008; Pour and Hashim. 2011).The technique employs the arithmetic combination of the different bands based on the absorption and emission of the materials under study (Drury 2001). The technique effectively reduces the correlation of inter bands in the multispectral data (Drury 1993).
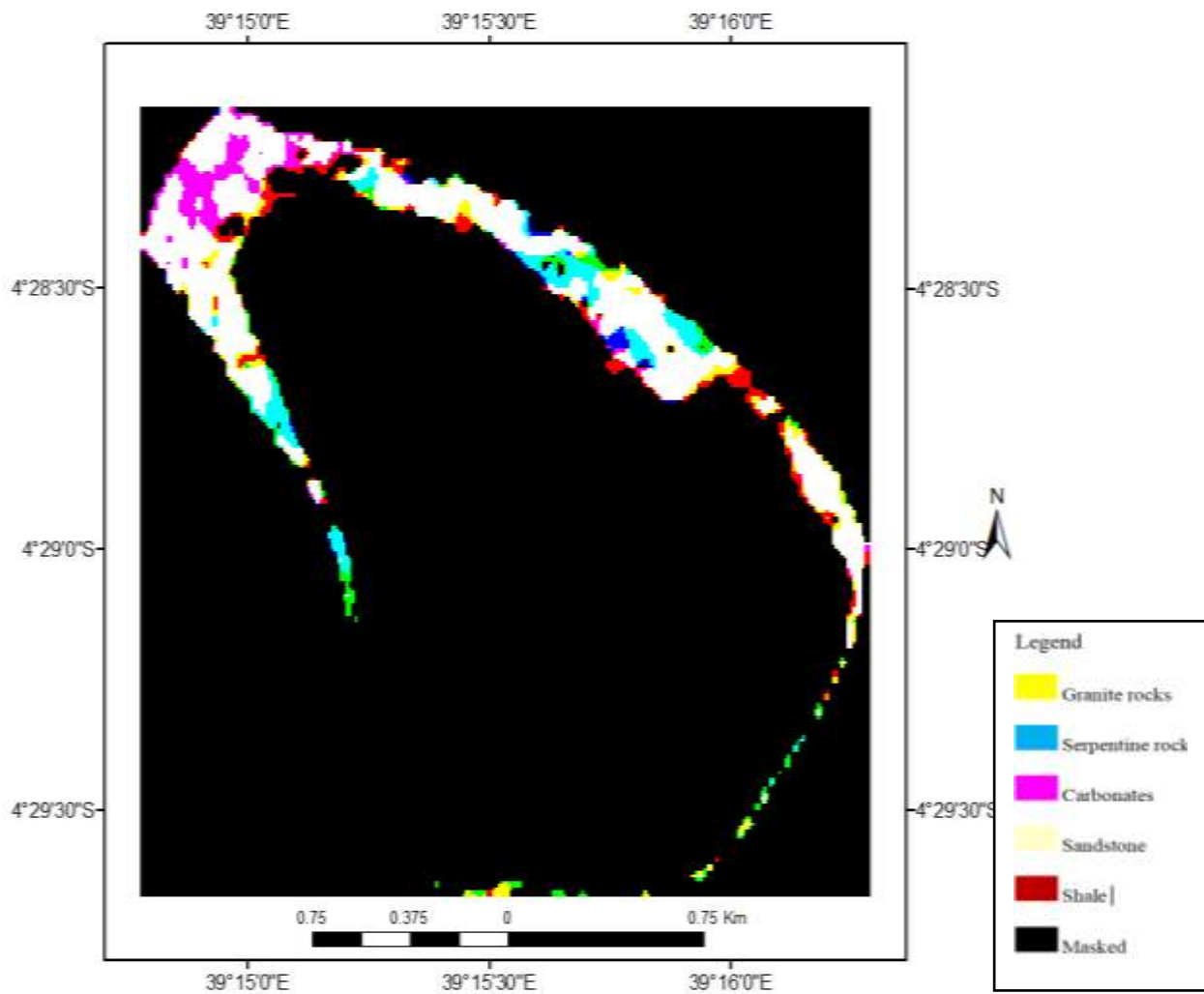

Figure 5.2: Landsat OLI ratio image (6/4, 7/3, 4/2 in RGB) for the study area

5.3   Rocks and Minerals: False color composite results

Figure 5.3 and 5.4shows the identified mineralized areas in the study area using FCC Landsat OLI image (bands 5, 6, 4; 7, 6, 5 in RGB).

Figure 5.5: shows identified different types of rocks associated with radioactive minerals in the study area using FCC Landsat OLI image (bands 7, 6, 2 in RGB).

This mapping technique employs the known spectral characteristics of minerals and rocks in relation to the bands selected. Three bands were used for lithological and alteration mapping in the case study. For carbonates and clay minerals, they have high absorption in band 7 and high reflectance in band 6. On the other hand, iron oxide minerals have high reflectance in band 4. Therefore, the band combination used to map these minerals was; band5, band 6 and band 4in RGB (Figure 5.3). The color composite of (5, 6, and 4) in RGB, therefore, highlights clay minerals in cyan while iron oxide minerals are highlighted by the red. The vegetation was masked out through the NDVI process by setting a threshold value of 0.25 and are therefore, shown by the black pixels in the image.
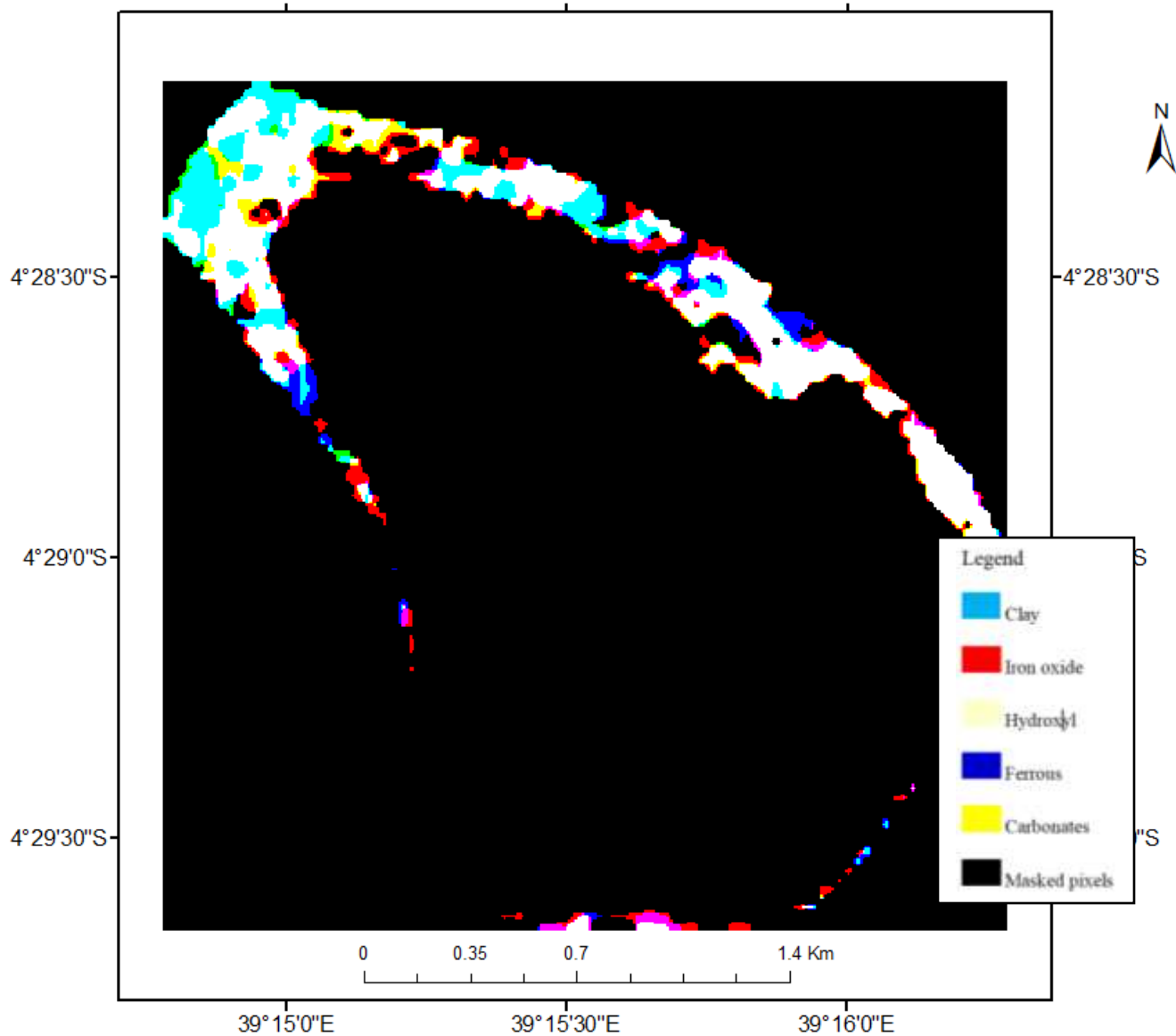
Figure 5.3: FCC Landsat OLI image (bands 5, 6, 4 in RGB) in the case study.

The combinations of bands 7, 6 and 5 for Landsat 8 in RGB were used to highlight the clay minerals by the yellow pixels since band 7 reacts to moisture contents and it's used in detecting hydrous minerals such as clay minerals. The bluish pixels represent the iron minerals because they have high reflectance in band 6 as shown in figure 5.4.
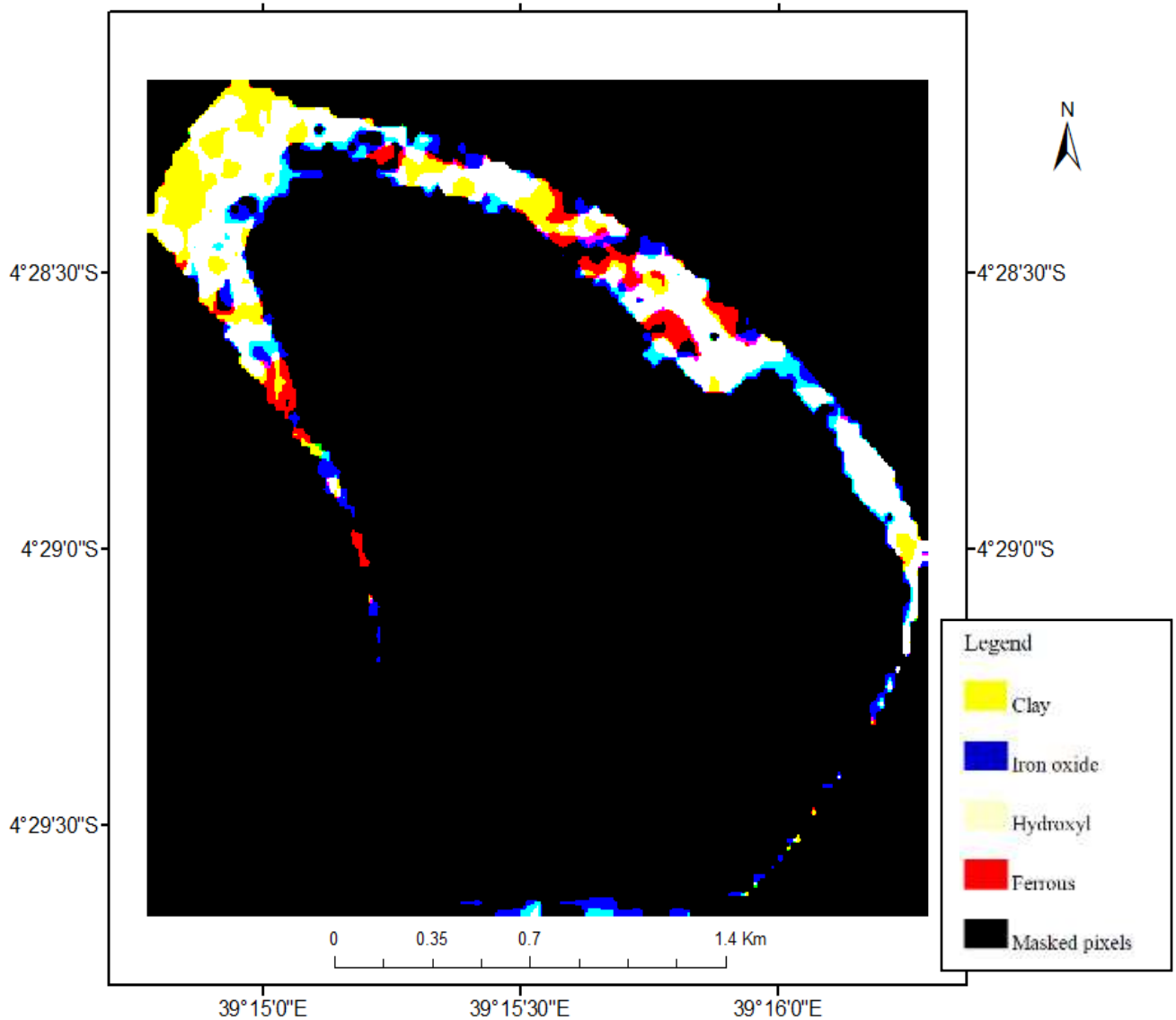
Figure 5.4: FCC Landsat OLI image (bands 7, 6, 5 in RGB) of the study area

The rocks associated with radioactive minerals were discriminated using the combination of 7, 6, and 2 for Landsat 8 data. This is because the granite rocks have high reflectance in band 7 while serpentine rocks have high reflectance in band 6. Therefore the combination of 762 in RGB show granite rocks represented by the white pixels while serpentine rocks are represented by the yellow pixels and the carbonates rocks by the red pixels as shown in figure 5.5.
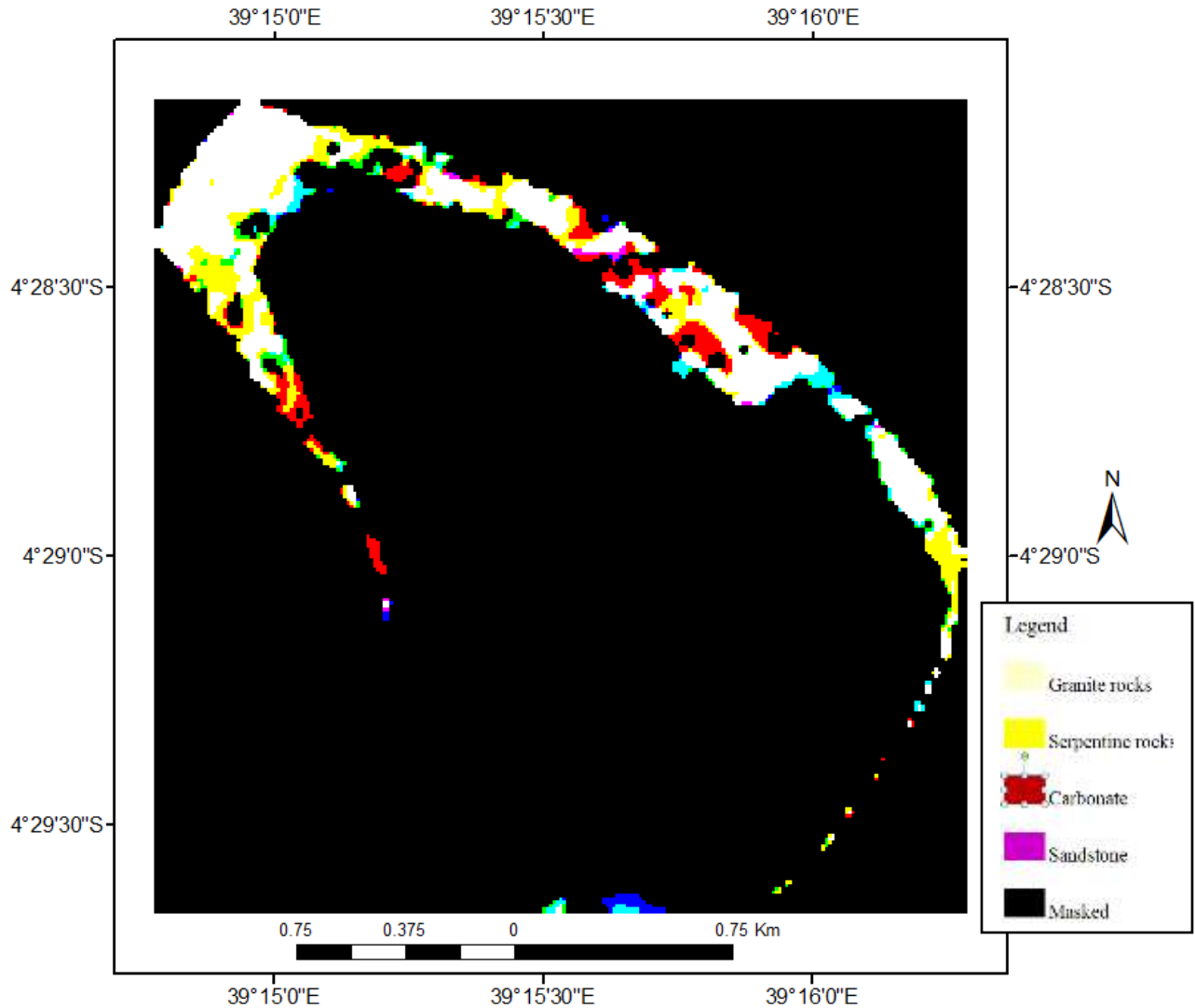
Figure 5.5: FCC for rocks Landsat OLI image (bands 7, 6, 2 in RGB) of the study area.

Good results of lithological mapping were achieved by the use of the color composite technique. Minerals such as jarosite, hematite, and limonite were mapped by using band 4 since they have high reflectance in this band. Clay minerals on the other hand, have high absorption in band 7 and high reflectance in band 6 (Han et al., 2015). Minerals such as alunite, and clay minerals such as illite, kaolinite and montmorillonite have distinctive absorption features at 2.20μm and low absorption at 1.6μm, hence, were calculated to map clay deposits in the study area.

5.4   Principal Component Analysis results

Figure 5.6 and 5.7 shows the results for iron oxide and clay minerals using PC4 and PC 2 images.

The principal component in this study was used to identify the minerals of interest by examining their eigenvector loadings. The iron oxide minerals that were identified were designated by bright pixels while the clay minerals were identified by the dark pixels as shown in figure 5.6 and 5.7.

PC transformation was applied to Landsat OLI image of the study area whose statistical analysis, eigenvalues, and eigenvector loadings were tabulated in table 5.1.

Table 5.1: Principal Component Analysis of OLI data

	PC1	PC2	PC3	PC4	PC5	PC6	PC7
BAND1	0.3469	-0.0565	-0.5073	0.3572	0.4014	-0.1138	-0.5634
BAND2	0.3171	-0.0782	-0.4347	0.1736	0.1077	-0.1190	0.8053
BAND3	0.2979	-0.0964	-0.2891	-0.0668	-0.4928	0.7501	-0.0916
BAND4	0.2674	-0.2341	-0.2097	-0.5155	-0.4523	0.5791	-0.1552
BAND5	0.6209	0.7101	0.2881	-0.1524	0.0611	-0.0174	0.0022
BAN6	0.3989	-0.4353	0.5406	0.5345	-0.2433	-0.1192	-0.0078
BAND7	0.2726	-0.4825	0.2257	-0.5130	0.5630	0.2456	0.0393
Variance %	92.3573	4.9614	1.9279	0.3225	0.2739	0.1108	0.0463
Cumulative %	92.3573	97.3187	99.2466	99.5691	99.843	99.9538	100

PC 1, PC2 and PC 3 accounts for 99.2466% of the total variance (table 5.1).The information about the minerals of interest is mostly found in these three PCs; PC1 and combined PC2and PC3, represents topography and vegetation of the study area, respectively.

In order to increase the probability of mapping iron oxide and clay bearing minerals, a combination of bands (2, 4,5 and 6) and (2, 5, 6 and 7), were selected respectively on the basis of high reflectance and high absorption for both iron oxide and clay minerals.

Table 5.2 shows the loadings of bands 4 and 2 on PC4, which are positive (reflectance) and negative (absorption), respectively for iron-oxides minerals. The iron oxide minerals were represented by dark pixels in PC4.

Table 5.2: Crosta Technique for Iron minerals

	PC1	PC2	PC3	PC4	VARIANCE%
BAND2	0.4969	0.7394	0.0304	-0.4532	95.1129
BAND4	0.4198	0.2141	-0.4075	0.7822	3.2504
BAND5	0.6267	-0.3772	0.6718	0.1169	1.3085
BAND6	0.4291	-0.5149	-0.6178	-0.4112	0.3281

On the other hand, hydroxyl-bearing minerals were highlighted as dark pixels in PC3 images because the eigenvector loadings of band 5 and band 6 were negative (absorption) and positive (reflectance) respectively. In order to enhance both iron oxides and the hydroxyl-bearing minerals, their respective PCs were made negative (DN multiplied by -1), such that these alteration minerals were mapped in brighter pixels as shown in figure 5.6 and 5.7.
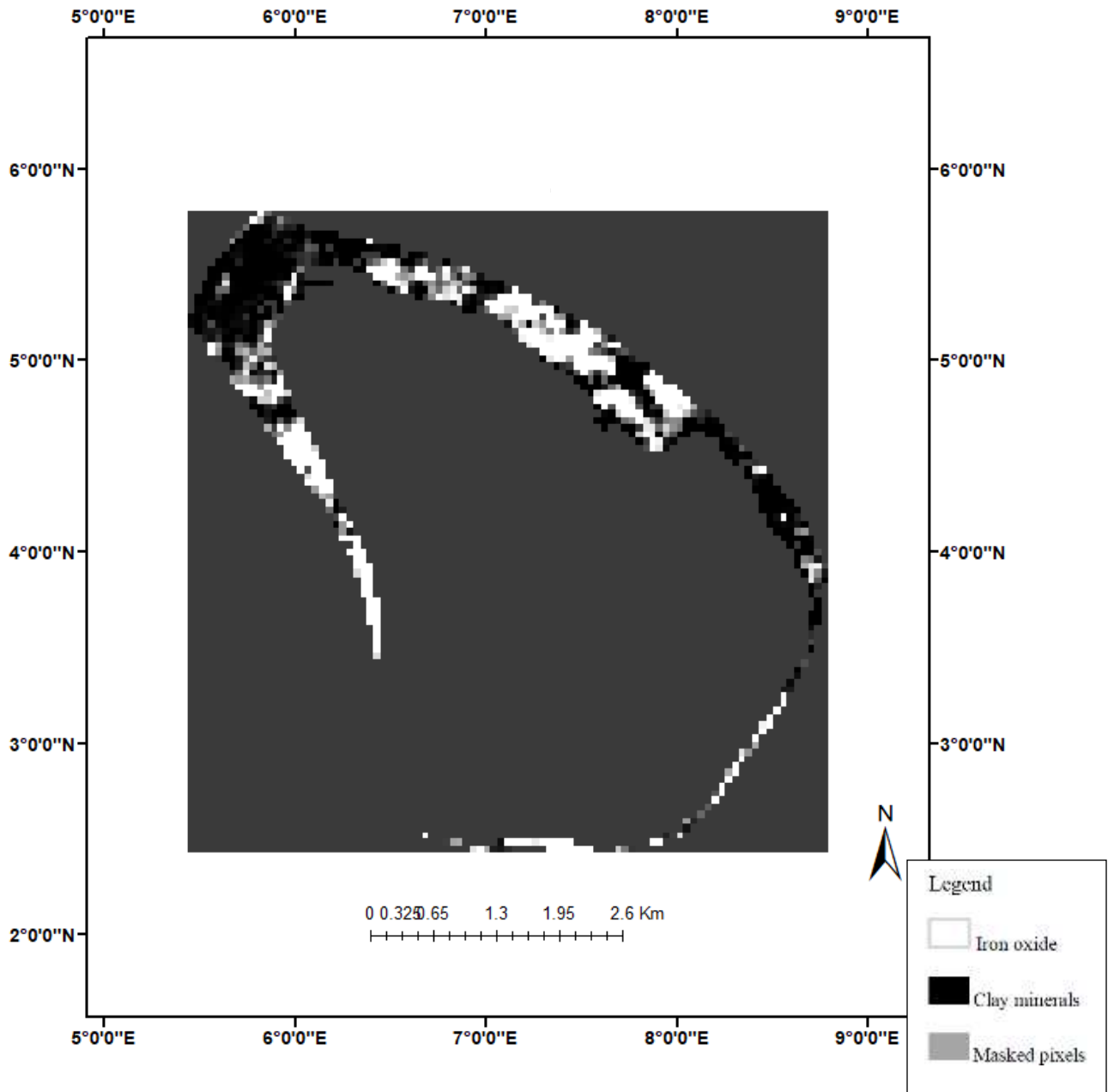
Figure 5.1: the PC4 image of iron minerals, with the bright pixels showing the areas of iron minerals.
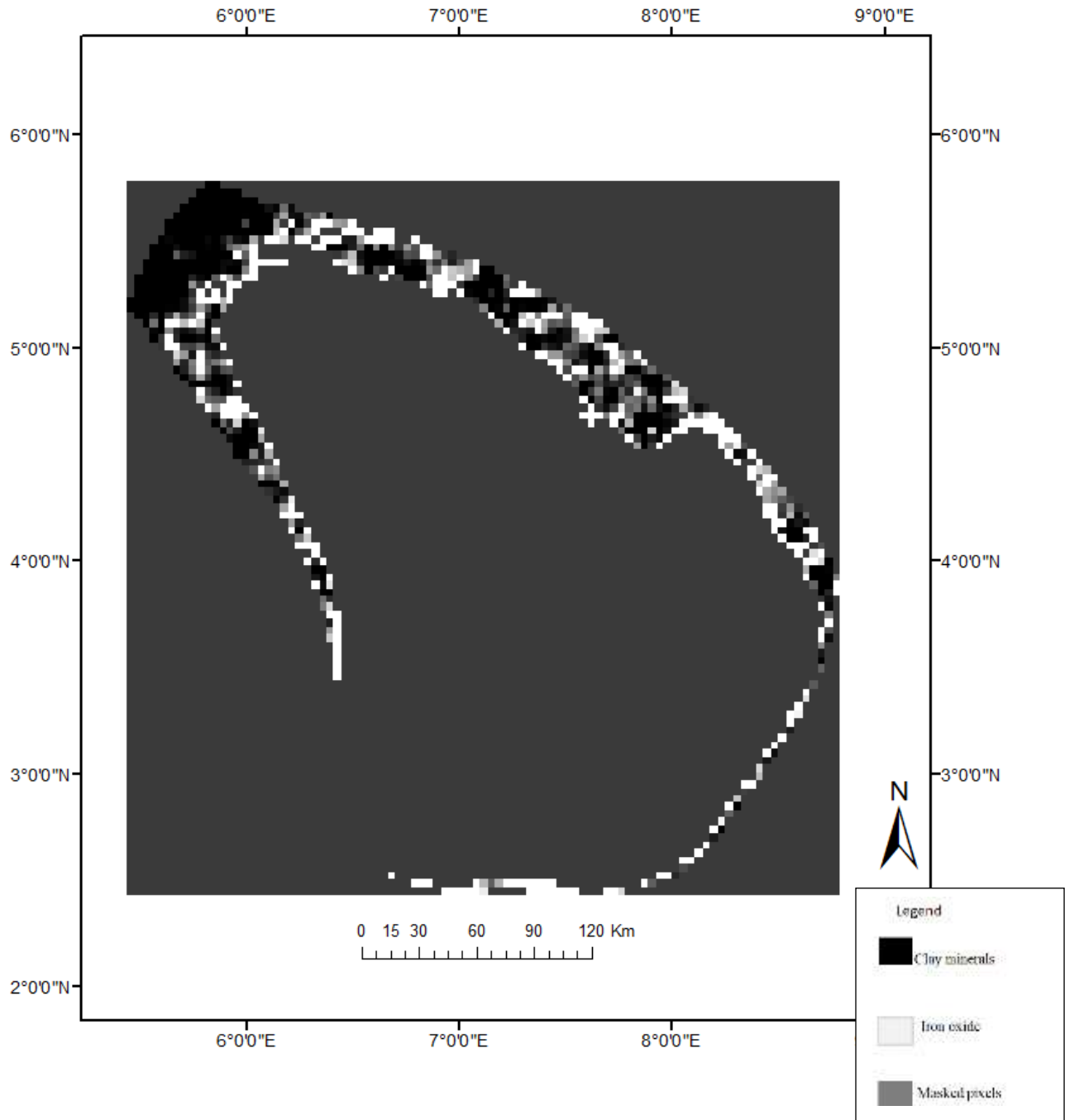
Figure 5.2: PCA2 image for clay minerals with dark pixels representing the clay minerals in the study area

In general, this technique utilizes the generalized reflectance curve of the material of interest, such as alteration zones of minerals in which bands are considered in the choice of the best Principal Component, based on their respective eigenvector loadings. For instance, to determine which PC best represent iron-bearing minerals depends on the eigenvector values of bands 4 and 2 in a Landsat OLI dataset. Likewise, the clay minerals are controlled by the eigenvector values

of bands 6 and 7 references to their generalized reflectance spectra curve of the USGS Library of minerals.

The signs (+/-) of the eigenvector value loadings are being considered in the process because they determine which component of interest (Fe oxide or clay) would be represented as bright or dark pixels in the image (E. Chuvieco et al.., 2010). In selecting the optimum principal component, the two loadings should always be different in signs.

The PCA was employed on selective bands and therefore, materials such as vegetation were not mapped and materials such as minerals were highlighted into a single PC. The PCs were selected based on the eigenvector loadings with the highest PCs being selected. For example, according to Crosta (2003), the high reflected and low reflected materials of interest bands and the corresponding eigenvectors loadings are checked to determine the PCA which has the needed information.

5.5   Rocks: Spectral Angle Mapper Results

Figure 5.8: shows the Spectral angle mapper classification results for rocks associated with radioactive minerals in the study area.

The results show that most of these rocks; granites, serpentine, carbonates, shale and sandstone identified in the study area were found at the edges of the hill (figure 5.8).The area was not covered by any vegetation and therefore, the signal response from the rocks could easily be recorded. However, the areas which had vegetation were masked out and are represented by the dark pixels.
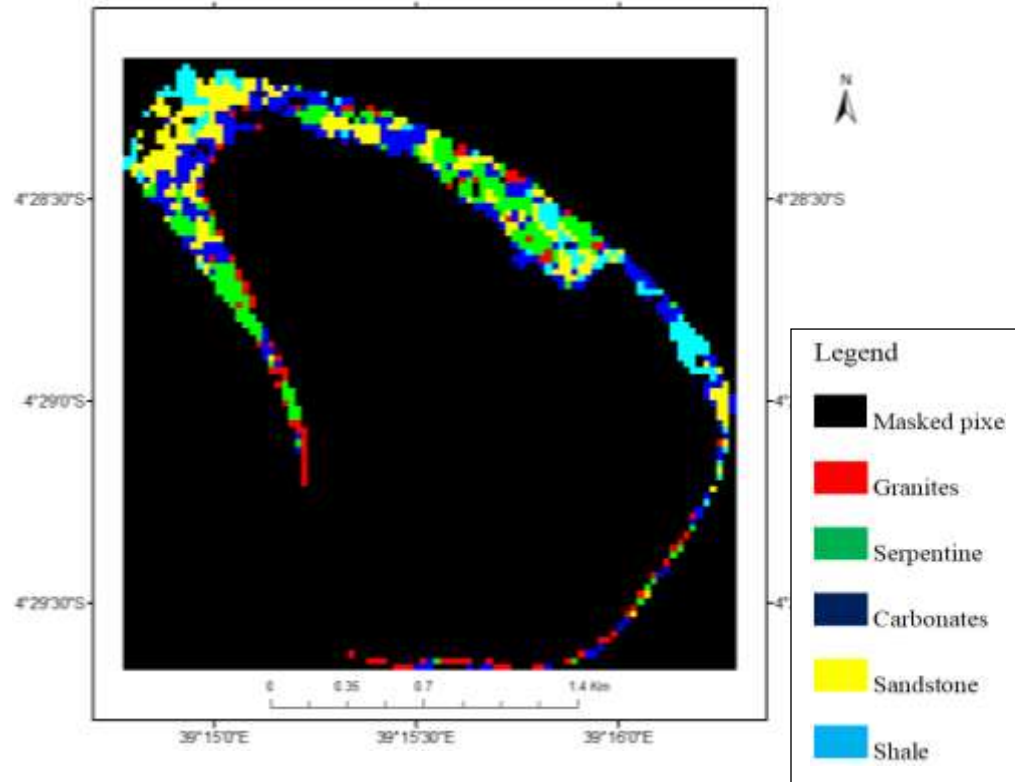
Figure 5.3: Spectral angle mapper classification for rocks associated with radioactive minerals in the study area.

In general, Spectral angle mapper classification was effective in mapping out the rocks associated with radioactive minerals in the study area. It was found out that alkali granite, sandstone, shale and carbonates rocks were identified in the study area. This is due to the fact that radioactive minerals; U, Th and rare earth metals are usually found in the sedimentary, metamorphic and magmatic rocks (Pavlidou et al, 2006) and are concentrated in acidic volcanic and plutonic rocks.

5.6   Rocks and Vegetation: Maximum Likelihood Classification Results

Figure 5.9 and 5.10 shows the results of Maximum Likelihood classification for rocks and botanical indicators for radioactive minerals in the study area.

The results obtained show that most of the rocks identified in the study area; granites, sandstone, carbonates and serpentine were located at the edges of the hill (figure 5.9). The areas where these

rocks were located were not covered by vegetation therefore; they had high probability of being classified since their signals could easily be recorded.
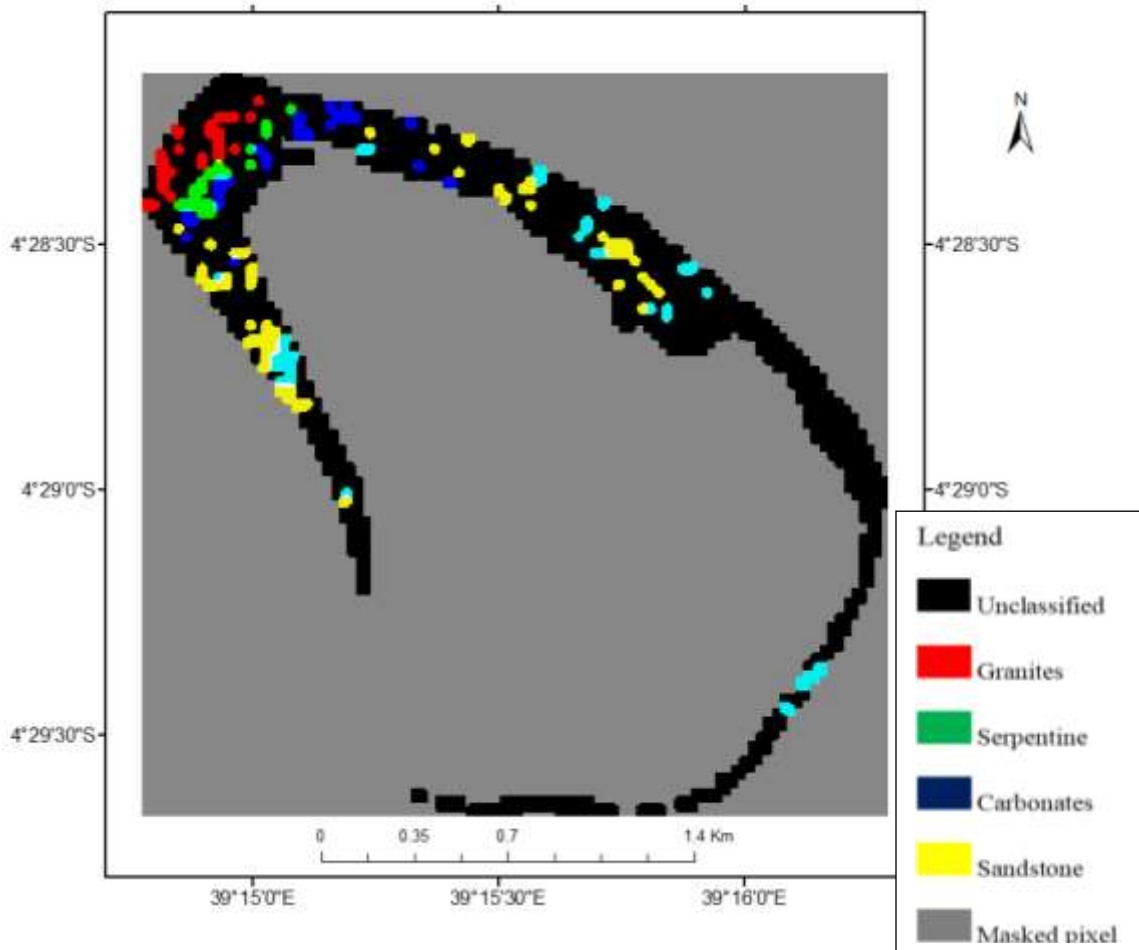

Figure 5.4: Maximum Likelihood classification for rocks associated with radioactive minerals in the study area.

Areas which were covered by vegetation could not be classified for rocks identification. The botanical method was used whereby the spectral signatures of vegetation associated with radioactive minerals were mapped. The vegetation used in this study were from *Astragalus* species, *Stanleya, Aster venustus, Oryzopsisj* species and they included Mormon tea, big berry Manzanita, big sagebrush, and pynon pine. This vegetation are bio indicators of selenium.
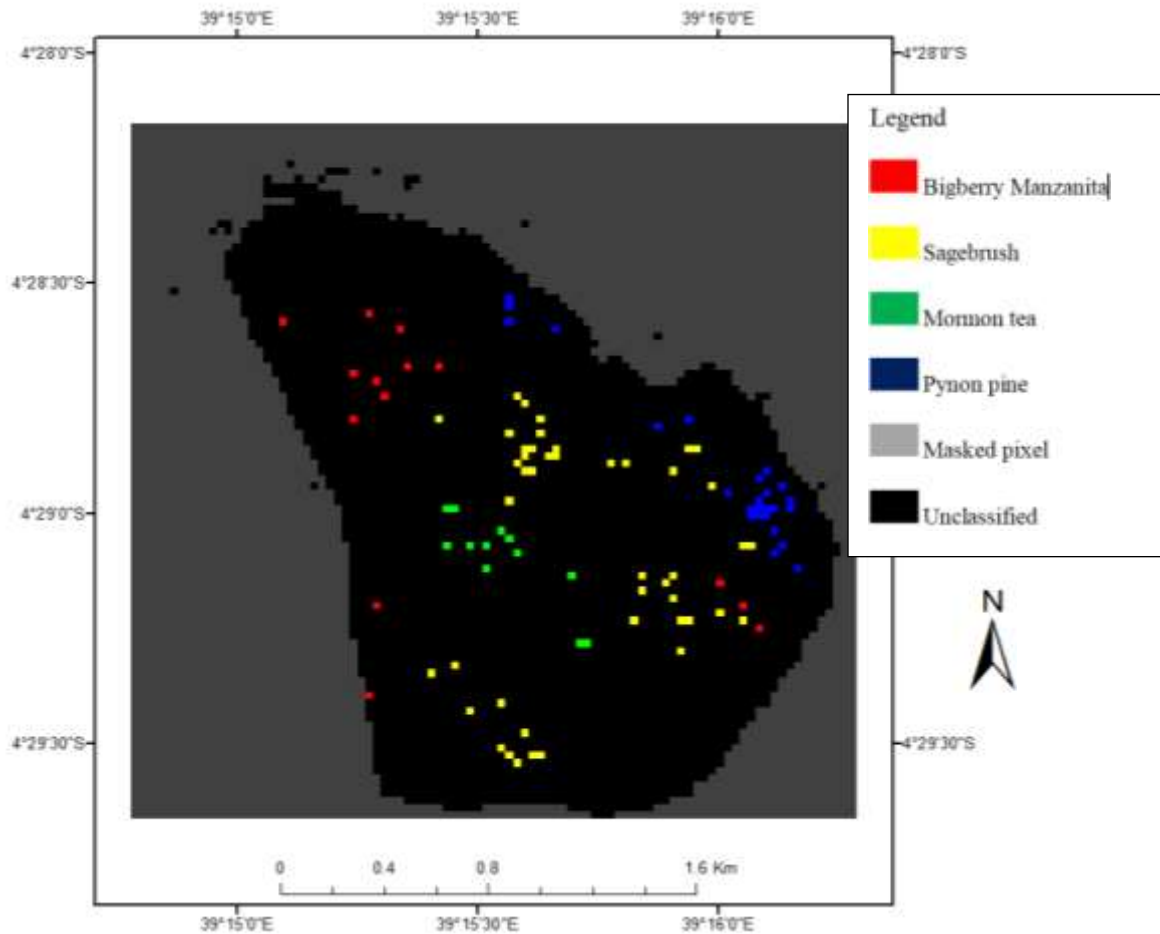
Figure 5.5: Maximum likelihood classification of vegetation associated with radioactive minerals

The geobotanical method was used in identifying radioactive minerals in the study area. These plants are bio indicators for radioactive minerals (Trelease and Beath, 1949).

In general, most uranium ores contain sulfides. Therefore gypsum is also a good indicator of uranium deposits. The distribution of sulfur and calcium absorbing plants indicate the presence of gypsum in the soil. Plants that require large amounts of these elements for their growth are indicators of radioactive minerals in the study area. Both of these indicators i.e. sulfur and selenium are normally found in the sedimentary, alkali granite, metamorphic and magmatic rocks but their concentration vary.

5.7 Validation of Remote Sensing Results using Existing Radiometric Survey Data: Comparison

The validity of the remote sensing results was determined by comparison of this data with the results of existing radiometric and geological data of the study area.

Figures 5.6a and 5.6b, 5.7a, 5.7b shows the remote sensing results of the study area using band ratio technique for rocks and minerals overlay over gamma dose rate and geological map of Mrima hill.

The comparison indicated similarity of minerals alteration zones and rocks for; clay, iron oxide, ferrous and hydroxyl minerals and granite, serpentine, carbonates and sandstone rocks for the location of threshold dose rate of over 600nGy/hr as shown by figure5.6a, 5.6b, 5.7a and 5.7b.
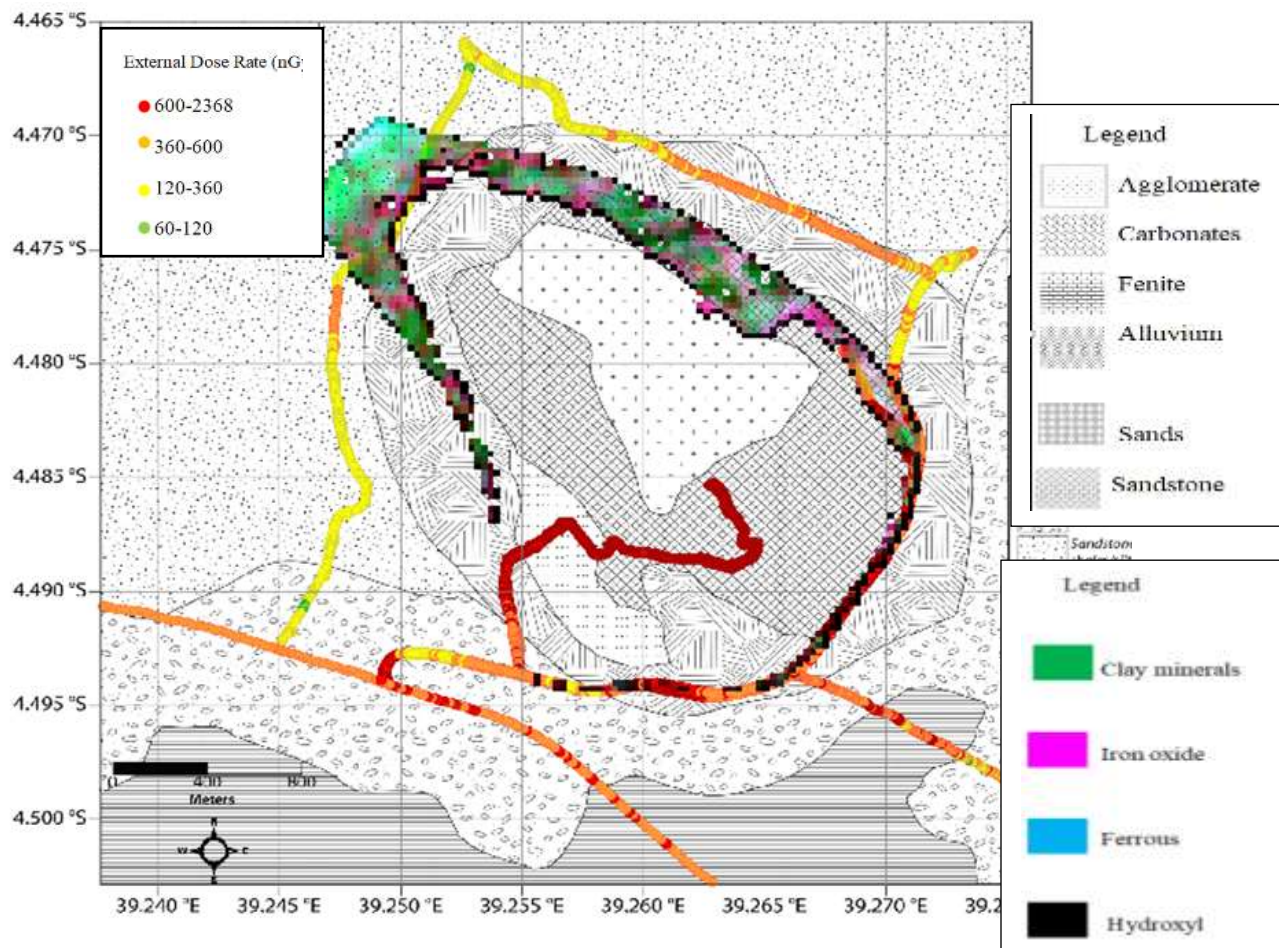

Figure 5.6a: Band ratio image of alteration mineral zones overlaid over gamma dose rate geological map of Mrima hill adapted from (Kaniu and Angeyo 2018)
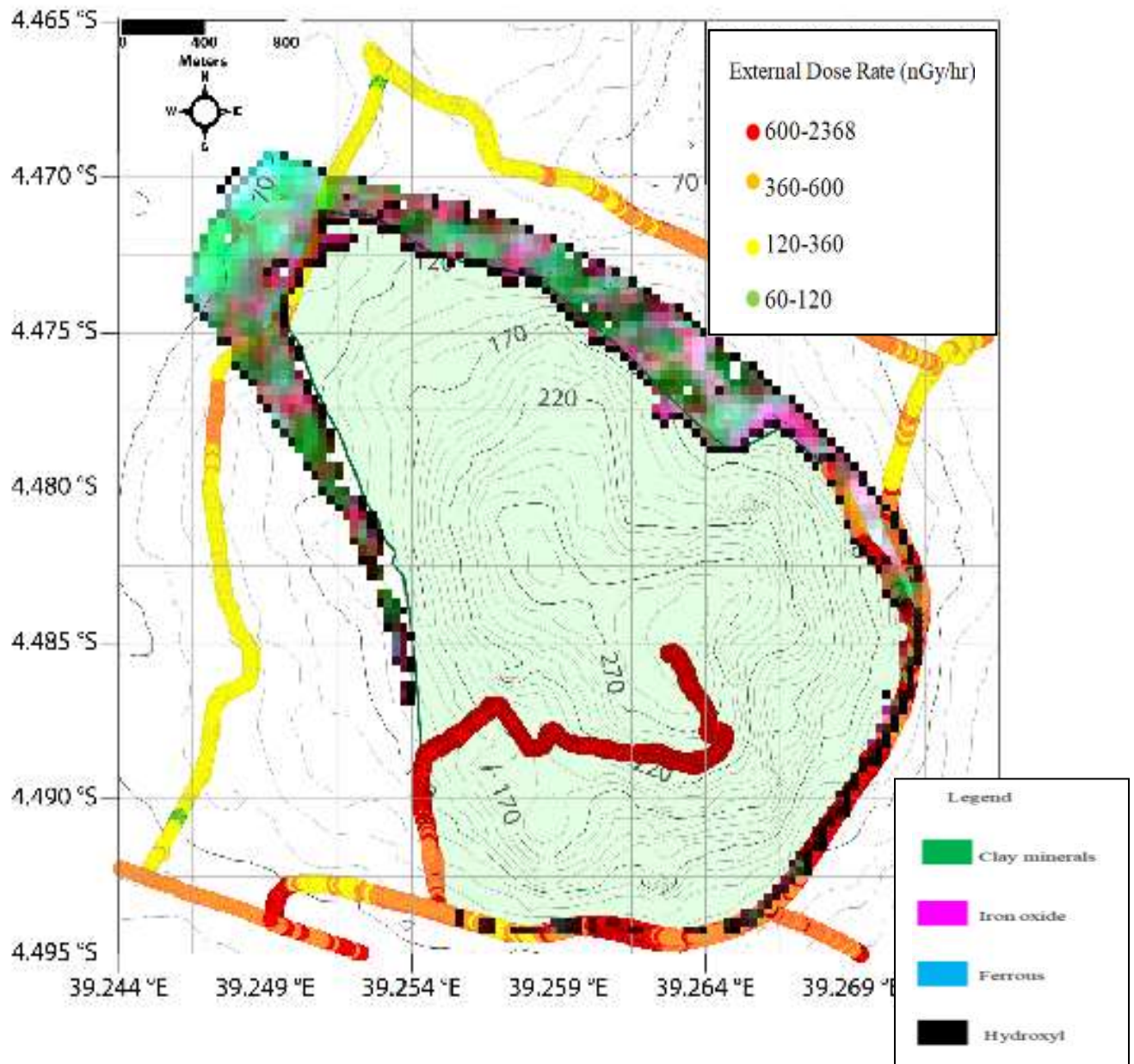
Figure 5.6b: Band ratio image of alteration mineral zones overlaid over gamma dose rate topographical map of Mrima hill adapted from (Kaniu and Angeyo, 2018)
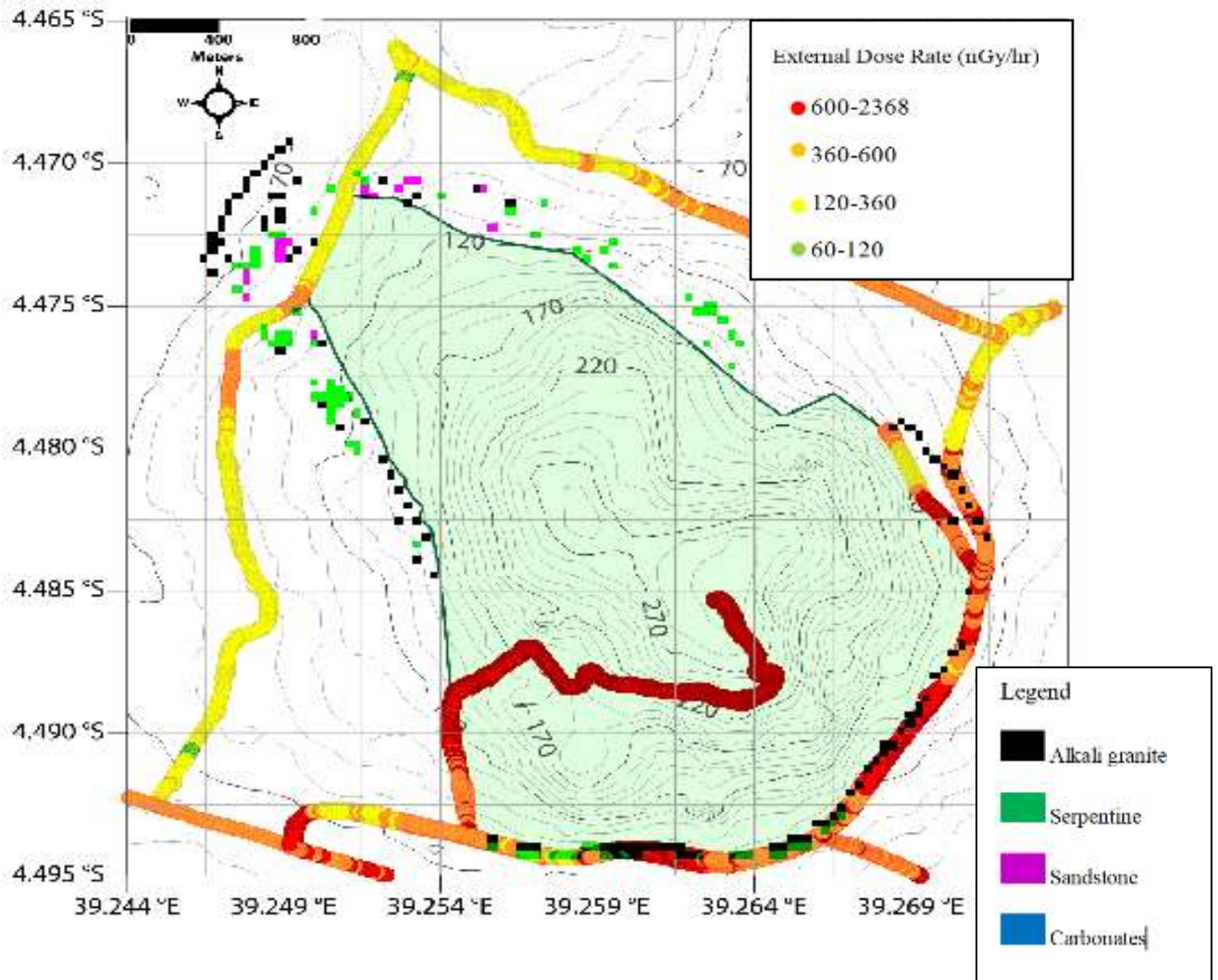
Figure 5.7a: Maximum likelihood classified image of rocks associated with radioactive minerals overlaid over gamma dose rate topographical map of Mrima hill adapted from (Kaniu, 2018).
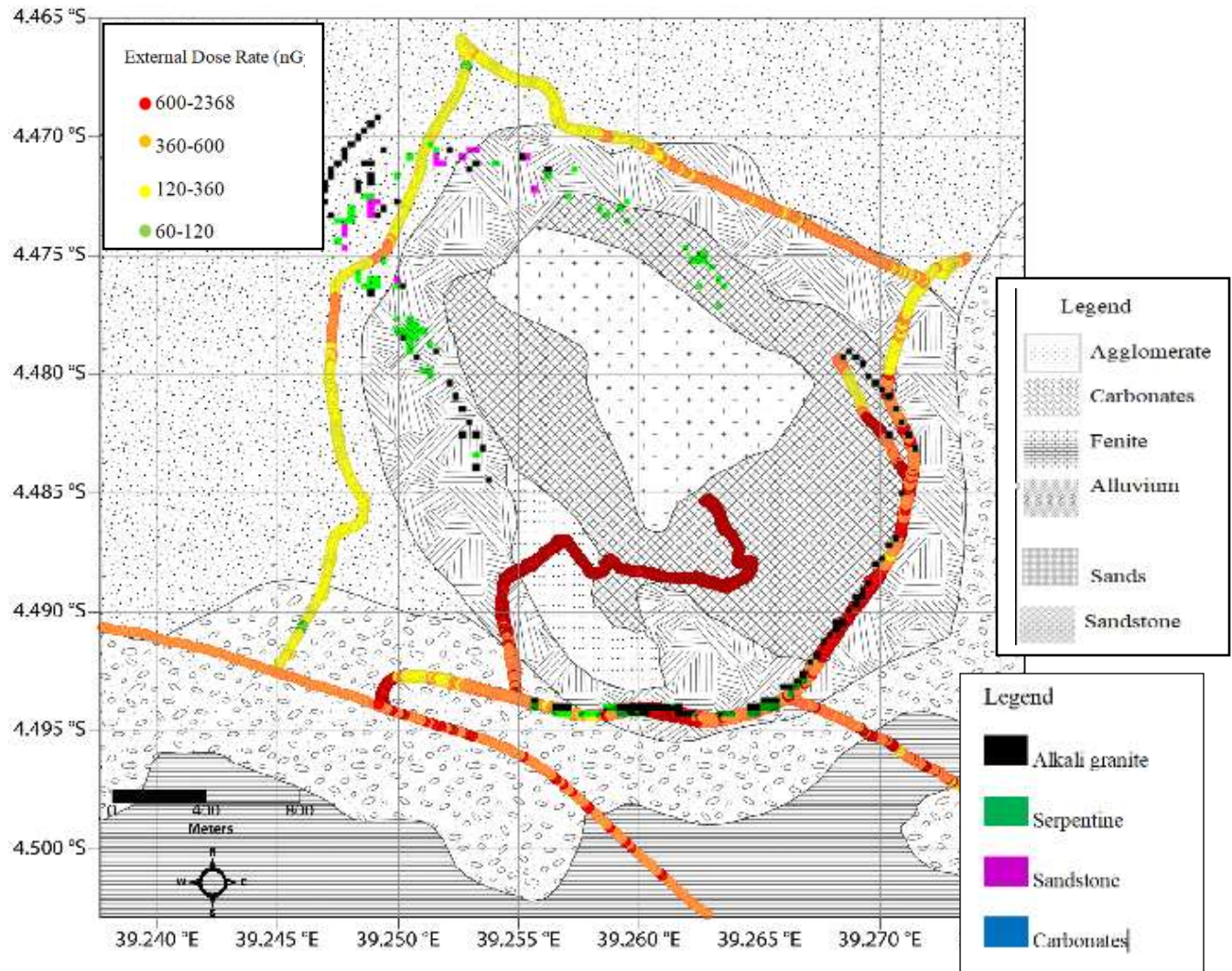
Figure 5.7b: Maximum likelihood classified image of rocks associated with radioactive minerals overlaid over gamma dose rate geological map of Mrima hill adapted from (Kaniu,2018).

In general, it was found out that the location for alteration minerals zones and rocks coincided with high radiation background areas.

It is observed that in Mrima hill, the hotspots were found in the crest of the hill and in the southern part of the hill. This is associated with colluvium and residual soils as well as carbonatite rocks according to the geology of the area (JICA, 1993). The eastern and northern part of the hill has low dose and are associated with sands, sandstone, shale and siltstones (Kaniu, 2017). These indicate the weathering of soil in the foothills of Mrima hill (Baker, 1993).

Figure 5.8 and 5.9 show the results of Maximum Likelihood classification of remote sensing data of vegetation associated with radioactive minerals overlay over interpolated gamma dose rate

map of Mrima hill. In these figures the existing radiometric data , was obtained from the southern part of the hill , however, radiometric data used for comparison with remote sensing data, had been interpolated to include areas that were inaccessible during the field survey(Kaniu, 2018).

Figure 5.8 shows the results of Maximum Likelihood classification of remote sensing data of vegetation associated with radioactive minerals overlaid over gamma dose rate map of Mrima hill.

The following vegetation; *bigberry manzanita, sagebrush, Mormon tea* and *pynon pine* were identified in the study area, to grow in areas with a threshold gamma dose rate of above 1200nGy/hr (figure 5.8).

When the same remote sensing data image was overlaid over radiometric data surveyed by Patel, (1991), the results indicated that the botanical indicator plants; *bigberry manzanita, sagebrush, Mormon tea* and *pynon pine*, were mostly concentrated in areas with a threshold dose rate of over 1386 nGy/hr (figure 5.9).

In addition, *Sagebrush* was dominant in areas with dose rate of above 800nSv/hr (gate 11, figure 5.10); *Bigberry Manzanita* was dominant in regions with dose rate of between 200nSv/hr and 800nSv/hr (gate 9, figure 5.10) while *pynon pine* was mostly found in region with dose rate of 50nSv/hr to 200nSv/hr (gate 16, figure 5.10).

The study area is considered to be hotspot and the high dose rate is attributed to the underlying geology of the area (Kaniu, 2017).The higher than the world average dose rate reported in other studies, has been attributed to the geological setting and presence of heavy mineral deposits for example, monazite (Veiga *et al*., 2006).

In general, selenium is found in areas with high background radiation and is highly associated with the botanical indicators for radioactive minerals (Trelease and Beath, 1949).

Plant communities may be definitive in outlining particular rock units such as limestone, sandstone, halite, or ultra basic rocks (Nicolls et al. 1965).
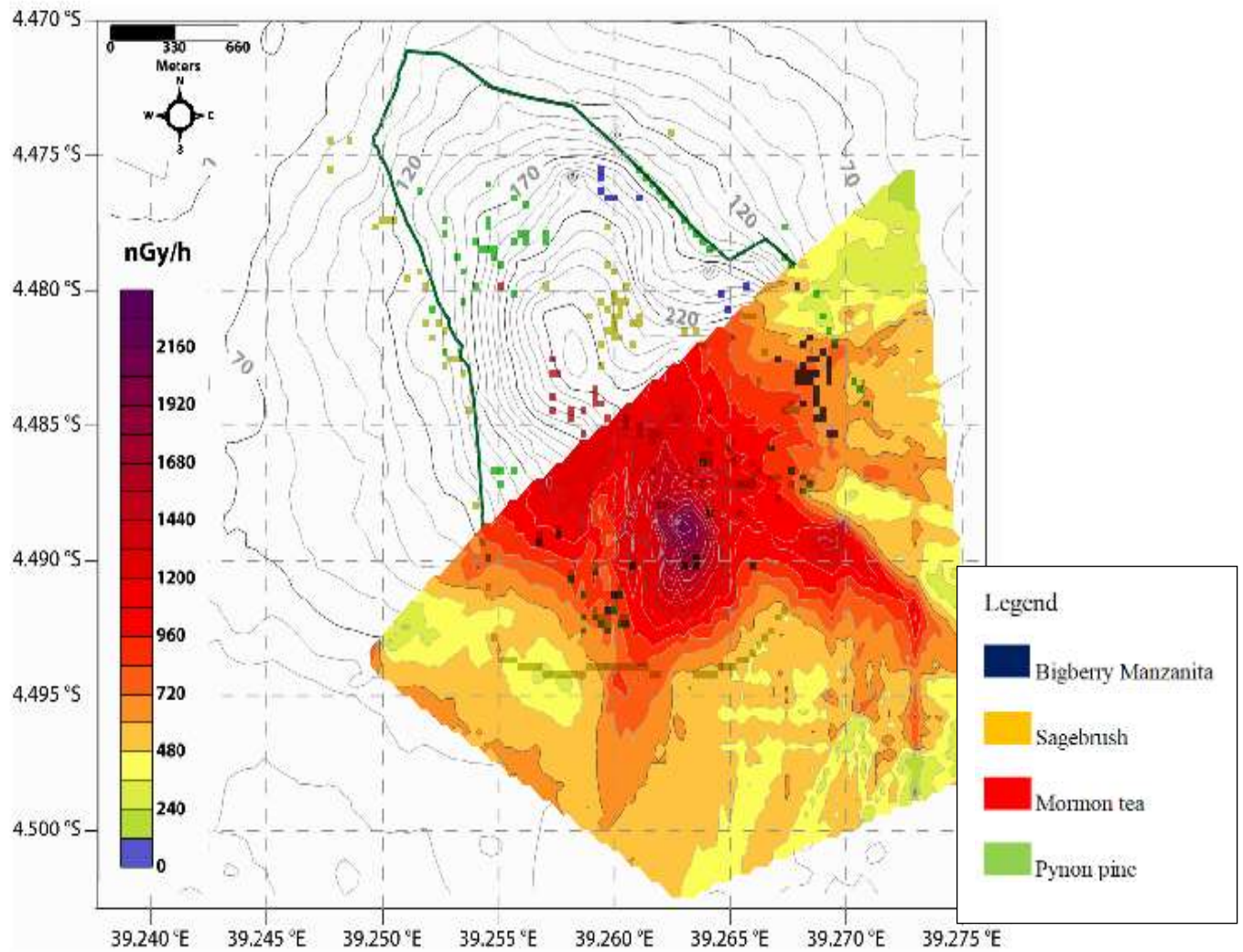
Figure 5.8: Maximum Likelihood classified image of vegetation associated with radioactive minerals overlaid over interpolated gamma dose rate map of Mrima hill adapted from (Kaniu, 2018).
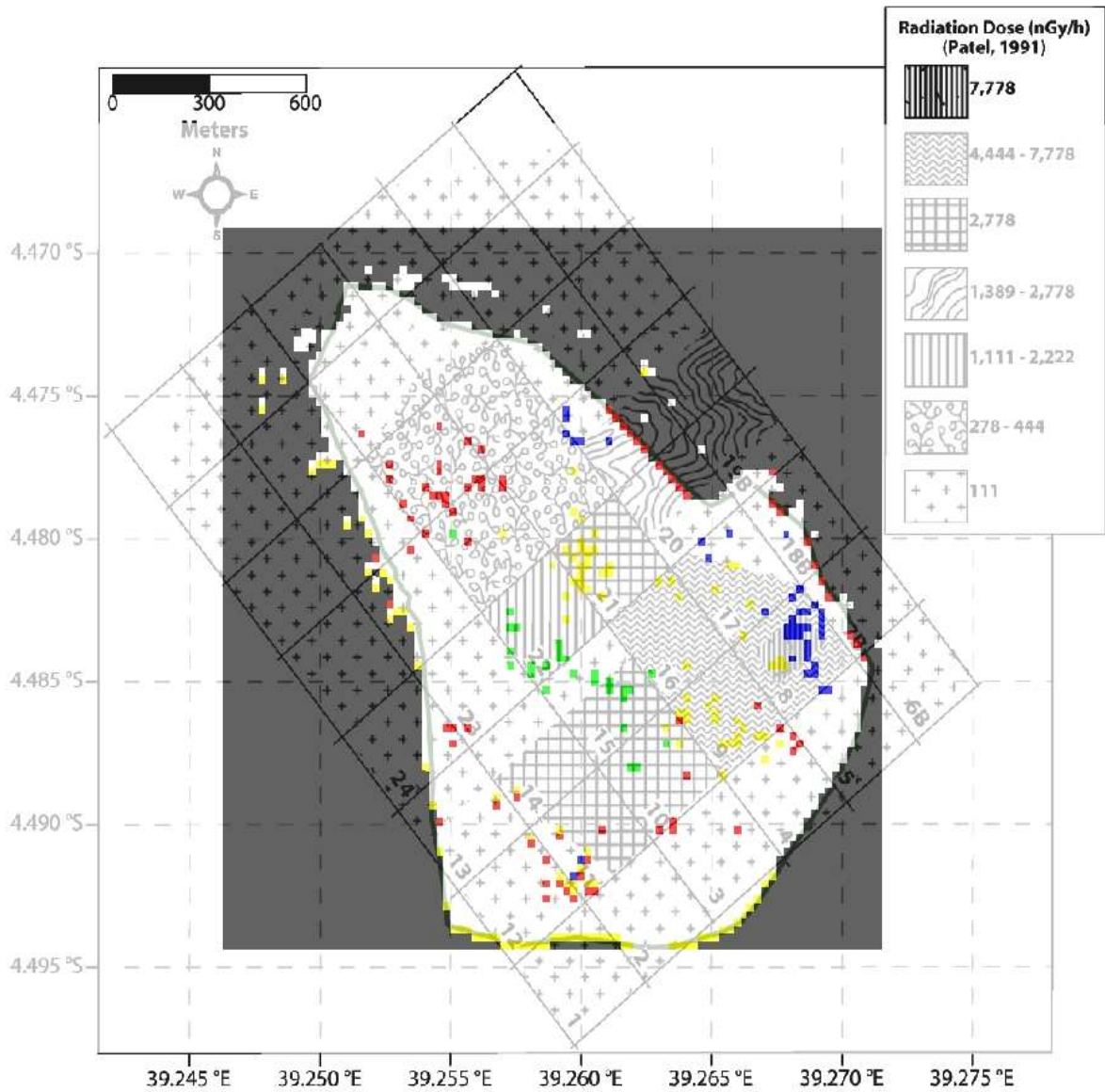
Figure 5.9: Maximum Likelihood classified image of vegetation associated with radioactive minerals overlaid over gamma dose rate map of Mrima hill adapted from (Patel, 1991).
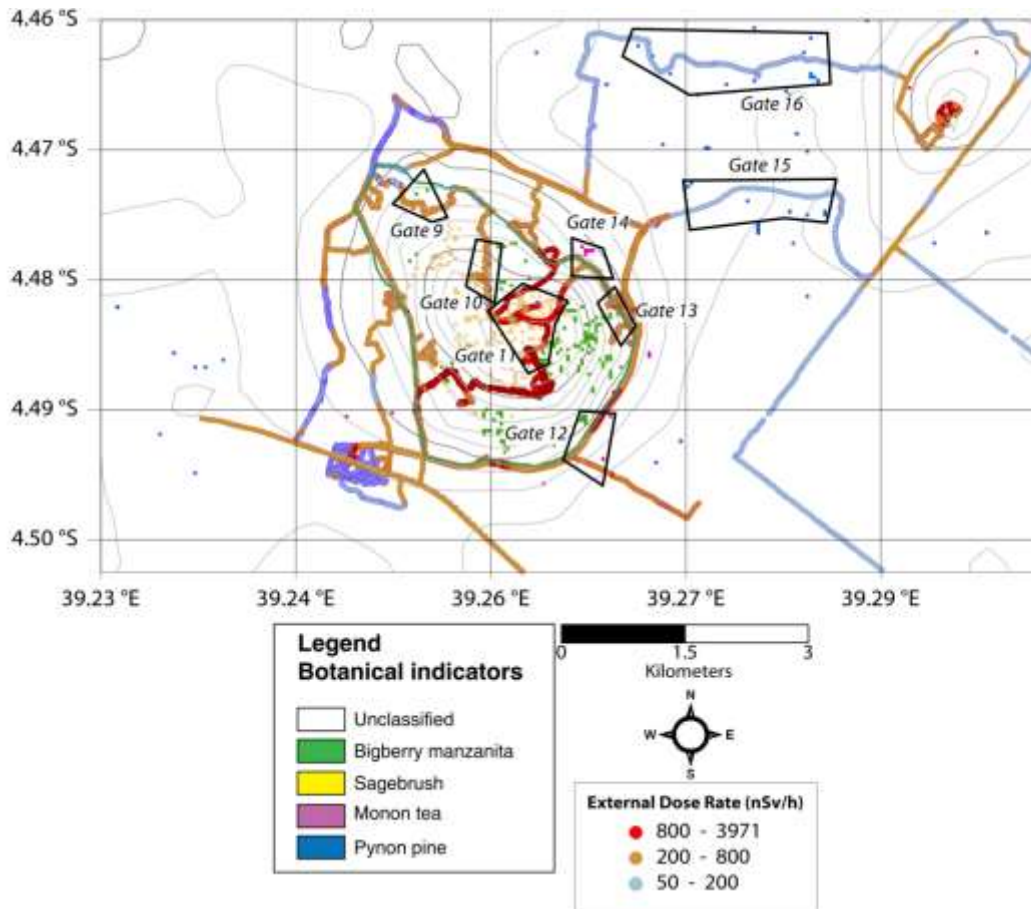
Figure 5.10: Maximum Likelihood classified image of vegetation associated with radioactive minerals overlaid over gamma dose rate map of Mrima hill adapted from (Ian, 2019)

5.8 Summary of the Findings of Remote Sensing Mapping Techniques

Radioactive minerals are effectively mapped using various remote sensing techniques depending on how effectively the spectral signatures of rocks and minerals are differentiated. Thus, each of the rock types has unique spectral signatures.

The color composite of 5, 6, and 4 in RGB identified altered zones of clay minerals and are separated from iron oxide minerals and carbonate minerals respectively. The technique helped in enhancing the geological features Bedini (2009).

As shown in figure 5.1, the altered clay and carbonatite minerals are identified as cyan and yellow pixels. This is because the clay and carbonatite minerals have high absorption in band 7 Clay and carbonatite minerals have high absorption in band 7 and high reflectance in band 6.

Therefore, clay and carbonate minerals have the same absorption and reflectance bands hence can be used to map both of them (Van der Meer, 2004; Zaini et al., 2016)

The band ratio of 6/4, 7/3, and 4/2 were used to identify the following rocks; granites, serpentine, sandstone, shale and carbonates, in the study area. This is because, granite rocks have high reflectance in band 7 of Landsat 8 and high absorption in band 3, while carbonates have high reflectance in band 4 and high absorption in band 2. The rocks are identified by the yellow, cyan, red, pink colors (figure 5.5).

The supervised classification method, which used training data for identification of rocks and vegetation, associated with radioactive minerals, were able to map following the rocks in the study area; granite, carbonates, sandstone and serpentine (figure 5.8 and 5.9). The following botanical indicators; *bigberry manzanita, sagebrush, Mormon tea and pynon pine* were identified in the study area (figure 5.10).

The validation with the existing radiometric data of the study area revealed that the areas with high dose rates coincided well with rocks and vegetation associated with radioactive minerals in the study area. The high dose rate is attributed to the underlying geology of the study area which is considered as hotspot as it contains masked radioactive minerals.

Chapter six: Conclusion and Recommendations

6.1   Conclusion

The use of Landsat 8 OLI datasets in image processing was useful in identification of rocks and vegetation associated with radioactive minerals and delineation of alteration zones in the study area. The selection of band combination performed was based on the characteristics of spectral of the material under study. The use of band ratio techniques (Vincent, 1997, Chica-Olmo et al., 2002; Gad and Kusky 2007) enabled lithologic and hydrothermal alteration mapping based on diagnostic spectral signatures of iron, clay and hydroxyl minerals. Generally, the band ratios R (4, 2), R (6, 5), and R (6, 7) were utilized for mapping ferric, ferrous, and clay minerals, respectively. The alteration zones in the study area were mapped by the use of Crosta technique.

The image analysis techniques which included spectral angle mapper, maximum likelihood were able to map rocks associated with radioactive minerals in the study area. This was possible in areas which were not covered by vegetation as these signatures were possible to be recorded by the sensor on Landsat 8. Areas which were covered by vegetation made it difficult to map the spectral reflectance of rocks associated with radioactive minerals. Botanical methods were employed whereby vegetation indicators for radioactive minerals were used.

Using the radiometric survey data for data validation, showed that maximum likelihood classification was the most effective method for mapping both rocks and vegetation associated with radioactive minerals in the study area.

6.2 Recommendations

The application of remote sensing for mapping radioactive minerals in Mrima hill Kwale County has been successful in mapping alteration zones and rocks associated with these radioactive minerals. Consequently, the following is recommended for adoption, following the findings of this study:

1) Application of remote sensing in other areas characterized by high radioactivity;
2) To use remote sensing technology in mapping other minerals in remote areas of poor accessibility.

For further research, the following is recommended:

1) Integration with other mineral exploration methods, such as geochemistry and geophysics, will improve the results of the present exploration approach;
2) To use remote sensing data with high spectral and spatial resolution;

References

Abdeen, M.M., Thurmond, A.K., Abdelsalam, M.G., Stern, R.J. (2002), "Use of TERRA ASTER band-ratio images for geological mapping in arid regions: the Neoproterozoic Allaqi suture, Egypt"' J. Remote. Sens. Space Sci. 5, 19–40.

Abuga, V.O (2013), Geophysical Investigation of Mbeu Iron Ore Deposit in Meru County using Gravity Method. M.Sc. Thesis. Kenyatta University, Kenya

ACHOLA, S.O. Radioactivity and elemental analysis of carbonatite rocks from parts of Gwasi area, South Western Kenya. M.Sc. thesis, University of Nairobi (2009)

Ahmed, S. & Amin, B. (2014). ''Lithological mapping and hydrothermal alteration using Landsat 8 data: a case study in Ariab mining district, red sea hills, Sudan.'' Intl. J. Basic and Appld. Sci., 3(3), 199- 208.

Alexander G and David H.R. (1997) Surface geochemical techniques in gemstone exploration at the Rockland Ruby Mine, Mangare area, SE Kenya, Journal of Geochemical Exploration,59(2); 87–98.

Alimohammadi M., Alirezaei S., Kontak D.J. (2015), "Application of ASTER data for exploration of porphyry copper deposits: A case study of Daraloo–Sarmeshk area, southern part of the Kerman copper belt, Iran", Ore Geology Reviews 70, 290–304.

Amer, R., Kusky, T.M., Ghulam, A. (2010), "Lithological mapping in the central eastern desert of Egypt using ASTER data", J. Afr. Earth Sci. 56 (2–3), 75–82.

Bakhit F S, Kassas I A. ''Distribution and statistical analysis of radioactivity of the basement rocks in Wadi Atalla-El Missikat area and correlation with the surrounding areas, Central Eastern Desert, Egypt.'' Ann Geol Survey Egypt 1992; (XVIII): 393-407.

Boleneus D E, Raines G L, Causey J D, Bookstrom A, Frost T P and Hyndman P C., (2001). ''Assessment method for epithermal gold deposits in northeast Washington State using weights-of-evidence GIS modeling,'' USGS Open-File Report, 01-501.

Cardoso-Fernandes, J.; Teodoro, A.C.; Lima, A. Potential of Sentinel-2 data in the detection of lithium (Li)-bearing pegmatites: A study case. In Proceedings of the SPIE, SPIE Remote Sensing, Berlin, Germany, 10–13 September 2018; Michel, U., Schulz, K., Eds.; SPIE: Bellingham, WA, USA, 2018; p. 15.

Cardoso-Fernandes, J.; Teodoro, A.C.; Lima, A. Remote sensing data in lithium (Li) exploration: A new approach for the detection of Li-bearing pegmatites. Int. J. Appl. Earth Obs. Geoinf. 2019, 76, 10–25.

Cardoso-Fernandes, J.; Teodoro, A.C.; Lima, A.; Roda-Robles, E. Evaluating the performance of support vector machines (SVMs) and random forest (RF) in Li-pegmatite mapping: Preliminary results. In Proceedings of the SPIE, SPIE Remote Sensing, Strasbourg, France, 9–12 September 2019; Schulz, K., Michel, U., Nikolakopoulos, K.G., Eds.; SPIE: Bellingham, WA, USA, 2019.

Chandrasekar, Anil Cherian, and Rajamanickam G V., 2001. ''An integrated mapping and data based system for Coastal placer concentration: A case study at Kallar Vembar coast, Tamil Nadu''. Inter. Arch.Photo.Rem.And Spat.Inf. Sci, 5th edition, pp.3445 (2001).

Crosta A, Moore J. ''Enhancement of Landsat Thematic Mapper imagery for residual soil mapping in SW Minas Gerais State, Brazil-A prospecting case history in greenstone belt terrain.''In Thematic Conference on Remote Sensing for Exploration Geology Methods, Integration, Solutions, 7 Th, Calgary, Canada 1990; pp. 1173-87.

Crosta A P, De Souza Filho C R, Azevedo F and Brodie C, (2003). ''Targeting key alteration minerals in epithermal deposits in Patagonia, Argentina, Using ASTER imagery and principal component analysis.'' International Journal of Remote Sensing, 24, pp. 42334240.

Crowley j, Brickey, Fand Rowan L., (1989). ''Airborne imaging spectrometer data of the Ruby Mountains, Montana: mineral discrimination using relative absorption band depth images. ''Remote sensing of environment, 29,121-134.

Dogan H M. (2008). ''Applications of remote sensing and Geographic Information Systems to assess ferrous minerals and iron oxide of Tokat province in Turkey.'' International Journal of Remote Sensing, 29,

Drury, S., (2001). Image interpretation in geology pp.290, Blackwell Science, USA.233.

Gad S. and Kusky T. (2007). ''ASTER spectral rationing for lithological mapping in the Arabian Nubian shield, the Neoproterozoic Wadi Kid area, Sinai, Egypt.'' Gondwana Research 11: 326-335.

Gabr S, Ghulam A, Kusky T, (2010). ''Detecting areas of high-potential gold mineralization using ASTER data.'' Ore Geol. Rev., 38: 59-69.

Gemusse, U.; Lima, A.; Teodoro, A. Pegmatite spectral behavior considering ASTER and Landsat 8 OLI data in Naipa and Muiane mines (Alto Ligonha, Mozambique). In Proceedings of the SPIE, SPIE Remote Sensing, Berlin, Germany, 10–13 September 2018; Michel, U., Schulz, K., Eds.; SPIE: Bellingham, WA, USA, 2018.

Gemusse, U.; Lima, A.; Teodoro, A. Comparing different techniques of satellite imagery classification to mineral mapping pegmatite of Muiane and Naipa: Mozambique. In Proceedings of the SPIE, SPIE Remote Sensing, Strasbourg, France, 9–12 September 2019; Schulz, K., Michel, U., Nikolakopoulos, K.G., Eds.; SPIE: Bellingham, WA, USA, 2019.

Griffiths P S, Curtis P A S, Fadul S E A, Scholes P D., (1987). ''Reconnaissance geological mapping and mineral exploration in northern Sudan using satellite remote sensing.'' Geol J 22: 225-249.

HEALTH RESEARCH FOUNDATION High background radiation areas (2000) http://www.taishitsu.or.jp/radiation/index-e.html

Hewson RD, Cudahy TJ, Huntington JF. IEEE Trans Geosci RemoteSens p. (2001). ''Geological and alteration mapping at Mt Fitton, South Australia, using ASTER satellite-borne data; pp. 724–726.

Hackman, B.D., Charsley, T.J., Kagasi, J., Key, R.M., Siambi, W.S and Wilkinson, A. F. (1989). "Geology of the Isiolo Area" Nottingham, Derry and Sons Limited.

Hoseinjani M, Tangestani, M H, (2011). ''Mapping alteration minerals using sub-pixel unmixing of ASTER data in the Sarduieh area, SE Kerman, Iran'' International Journal of Digital Earth, DOI: 10.1080/17538947.2010.550937.

Holben B N. (1986). ''Characteristics of maximum-value composite images of temporal AVHRR data.'' Int. J. Remote Sens. 7: 1417-1434.

Hurcom S J, & Harrison A R. (1998). ''The NDVI and spectral decomposition for semi-arid vegetation abundance estimation.'' International Journal of Remote Sensing, 19, 3109 – 3125.

Hosseinjani Zadeh, M., Tangestani, M.H., Velasco Roldan, F., Yusta, I. (2013), "Mineral exploration and alteration zone mapping using mixture tuned matched filtering approach on ASTER data at the central part of Dehaj-Sarduiyeh copper belt SE Iran", IEEE Sel. Top. Appl. Earth Obs. Remote Sens.

Hosseinjani Zadeh, M., Tangestani. M.H., Roldan. F.V., Yusta. I. (2014a), "Spectral characteristics of minerals in alteration zones associated with porphyry copper deposits in the middle part of Kerman copper belt, SE Iran", Ore Geology Reviews 62, 191–198.

Hosseinjani Zadeh M., Tangestani M.H., Roldan F.V., Yusta I. (2014b), "Sub-pixel mineral mapping of a porphyry copper belt using EO-1 Hyperion data", Advances in Space Research 53, 440–451.

Hosseinjani Zadeh, M.; Honarmand, M. A remote sensing-based discrimination of high- and low-potential mineralization for porphyry copper deposits; a case study from Dehaj–Sarduiyeh copper belt, SE Iran. Eur. J. Remote Sens. 2017, 50, 332–342

Hunt G R, Salisbury J W, and Lehnoff C J, (1971). "Visible and near infrared spectra of minerals and rocks: III. Oxides and Ox hydroxides," Modern Geology, 2:195-205.

J.Aboelkhair, Yoshiki N, Yasushi, and Isao Processing and granitoids in the Central Eastern Desert of Egypt. J. Afri. Earth Sc. Article in press (America).

Jung M, Churkina G, Henkel K..,(2006). "Exploiting synergies of global land cover products for carbon cycle modeling." Remote Sens Environ 101:534-53.

Kaniu, M.I., (2017). "Rapid In-Situ Gamma-Ray Spectrometry and Associated Radiometric Assessment of the Mrima-Kiruku Complex (Kenya) High Background Radiation Anomaly." Ph.D. thesis. University of Nairobi (unpublished).

Kaniu, M. I., & Angeyo, K. H. (2018b). "Occurrence and multivariate exploratory analysis ofthe natural radioactivity anomaly in the south coastal region of Kenya." *Radiation Physics and Chemistry, 146*, 34–41.

Kaniu, M.I., Angeyo, H.K., Darby, I.G., Muia, L.M., (2018a). "Rapid in-situ radiometric assessment of the Mrima-Kiruku high background radiation anomaly complex of Kenya." J. Environ. Radioact. 188, 47–57

Kruse F A. (1993). ''The spectral image processing system (SIPS)-Interactive visualization and analysis of imaging spectrometer data.'' Remote Sens. Environ. vol. 44, pp. 145-163.

Lambert, M.P. (1994). ''Ionizing radiation associated with the mineral collection of the National Museum of Wales.'' Collection Forum. Vol. 10(2) pp.65-80.

Langley S K, Cheshire H M, Humes K S, (2001). ''A comparison of single date and multitemporal satellite image classifications in a semi-arid grassland.'' J Arid Environ 49:401-11.

Legg C V. (1994). ''Remote Sensing and Geographic Information Systems: Geological mapping, mineral exploration and mining:'' John Willey & Sons and Praxis Publishing LTD, p. 59.

Lillesand T M and Kiefer, R.W, (2000). ''Remote Sensing and image interpretation,'' 4rd edition, John Willey and sons, New York, 724p.

Liu F, Wu X, Sun H, Guo Y.,(2007). ''Alteration information extraction by applying synthesis processing techniques to Landsat ETM+ data: case study of Zhaoyuan Gold Mines, Shandong Province, China.'' Journal of China University of Geosciences 18, 72-76.

Liu L, Zhuang D F, Zhou J and Qiu D S., (2011). ''Alteration mineral mapping using masking and Crosta technique for mineral exploration in mid-vegetated areas: A case study of Areletuobie, Xinjiang (China).'' International Journal of Remote Sensing, paper 32, 1931-1944

Lo C P, Quattrochi D A, and Luvall J C., (1997). ''Application of high-resolution thermal infrared remote sensing and GIS to assess the urban heat island effect,'' International Journal of Remote Sensing, 18, 287 – 304.

Loughlin W P., (1991). ''Principal component analysis for alteration mapping.'' Photogrammetric Engineering and Remote Sensing 57, 1163-1169.

Massironi M L, Bertoldi P, Calafa D, Visona A, Bistacchi C, Giardino A, and Schiavo B, (2008). ''Interpretation and processing of ASTER data for geological mapping and granitoids detection in the Saghro massif (eastern Anti-Atlas, Morocco),'' Geosphere, 4(4): 736-759.

Mshiu E. (2011). ''Landsat remote sensing data as an alternative approach for geological mapping in Tanzania: A case study in the Rungwe volcanic province, south-western Tanzania,'' Tanzania Journal of Science, vol. 37, no. 1, 2011

Rajendran, S., Nasir, S. (2017), ''Characterization of ASTER spectral bands for mapping of alteration zones of Volcanogenic Massive Sulphide (VMS) deposits.'' Submitted to the Ore Geology Review.

Rajendran. S. (2016), "Mapping of Neoproterozoic source rocks of the Huqf Super group in the 3 Sultanate of Oman using remote sensing", Ore Geology Reviews. 78, 281-299.

Rajendran, S., Nasir, S. (2014a), "Hydrothermal altered serpentinized zone and a study of Ni magnesioferrite– magnetite–awaruite occurrences in Wadi Hibi, Northern Oman Mountain: discrimination through ASTER mapping", Ore Geol. Rev. 62, 211–226.

Rajendran, S., Nasir, S. (2015a), "Mapping of high pressure metamorphics in the As Sifah region, NE Oman using ASTER data", Adv. Space Res. 55 (4), 1134–1157.

Rajendran, S., Nasir, S. (2015b), "Mapping of Moho and Moho Transition Zone (MTZ) in Samail ophiolites of Sultanate of Oman using remote sensing technique", Tectonophysics 657, 63–80.

Ramadan T M, El Leithy B S. (2005). ''Application of airborne radiometric data and Landsat TM imagery in exploration for the mineralization in El Qasia-Umm Naggat granites, Central Eastern Desert, Egypt.'' Jour. Remote Sensing & Space Sci. 8, 143– 160.

Ramadan T M, Ibrahim T M, Said A D and Baiumi M., (2013). ''Application of Remote Sensing in Exploration for Uranium Mineralization in Gabal El Sela Area, South Eastern Desert, Egypt.'' The Egyptian Journal of Remote Sensing and Space Sciences, 16, 199-210.

Rajesh H M, (2004). ''Application of remote sensing and GIS in mineral exploration resource mapping- An Overview.'' Journal of Mineralogical and Petrological Sciences, 99: 83-103.

Richards J A., (1995). ''Remote sensing, Digital Image Processing, an Introduction,'' Sec.Ed. Springer Velag. P. 340.

Rokos D, Mavrantza R, Vamvoukakis K , St-Seymour, Kouli M, Karfakis I and Denes G .,(2000). ''Localization of ore alteration zoning for the detection of epithermal gold by

integration of remote sensing and geochemical techniques:'' Proceedings of the Fourteenth International Conference on Applied Geologic Remote Sensing, Las Vegas Nevada, p. 161-168.

Rowan, L.C., Mars, J.C. (2003), "Lithologic mapping in the Mountain Pass area, California using Advanced Spaceborne Thermal Emission and Reflection Radiometer (ASTER) data", Remote Sens. Environ. 84 (3), 350–366.

Sabins F., (1999). ''Remote sensing for mineral exploration,'' Ore Geology Reviews, 14: 157183.

Santos, D.; Teodoro, A.; Lima, A.; Cardoso-Fernandes, J. Remote sensing techniques to detect areas with potential for lithium exploration in Minas Gerais, Brazil. In Proceedings of the SPIE, SPIE Remote Sensing, Strasbourg, France, 9–12 September 2019; Schulz, K., Michel, U., Nikolakopoulos, K.G., Eds.; SPIE: Bellingham, WA, USA, 2019.

Shalaby M H, Bista A Z, Roz M E and El Zalaky M A.,(2009). ''Integration of Geologic and Remote Sensing Studies for the discovery of Uranium Mineralization in Some Granite Plutons, Eastern Desert,'' Egypt Journal of Earth Science, 1, pg. 1-25.

Pavlidou S, Koroneos A, Papastefanou C, Christofides G, Stoulos S, Vavelides M. ''Natural radioactivity of granites used as building materials.'' J Environ Radioact 2006; 8: 1-13.

Pour, A.B., Hashim, M. (2015), "Hydrothermal alteration mapping from Landsat-8 data, Sar Cheshmeh copper mining district, south-eastern Islamic Republic of Iran", Journal of Taibah University for Science 9, 155–166.

Volesky J C, Stern R J, Johnson P R., (2003). ''Geological control of massive sulfide mineralization in the Neoproterozoic Wadi Bidah shear zone, southwestern Saudi Arabia, inferences from orbital remote sensing and field studies.'' Preca. Res., 123 (24): 235-247.

Wilde, A.; Otto, A.; Jory, J.; MacRae, C.; Pownceby, M.; Wilson, N.; Torpy,. (2013). ''Geology and Mineralogy of Uranium Deposits from Mount Isa, Australia:'' Implications for Albitite Uranium Deposit Models, 3, 258–283.

Zhang X, Pamer, M & Duke N., (2007). ''Lithological and mineral information extraction for gold exploration using ASTER data in the South Chocolate Mountains (California).'' ISPRS Journal of Photogrammetry and Remote Sensing, 62, 271−282.

Appendix 1: MATLAB scripts for Principal Component Analysis for seven Bands of Landsat OLI data

```
Image=double (imread ('C: \Program Files\MATLAB\LANDSAT
IMAGES\mrimamaskedimage.tif'));

X = reshape (image, [], 7);

band2=image (: 1);

band3=image (: 2);

band4=image (: 3);

band5=image (: 4);

band6=image (: 5);

band7=image (: 6);

m2=mean2 (band2 (:))

m3=mean2 (band3 (:))

m4=mean2 (band4 (:))

m5=mean2 (band5 (:))

m6=mean2 (band6 (:))

m7=mean2 (band7 (:))

s2=std2 (band2)

s3=std2 (band3)

s4=std2 (band4)

s5=std2 (band5)

s6=std2 (band6)

s7=std2 (band7)
```

```
v2=var (band2 (:))

v3=var (band3 (:))

v4=var (band4 (:))

v5=var (band5 (:))

v6=var (band6 (:))

v7=var (band7 (:))

Disp ('......................................................................');

Covariance=cov(X)

 [v, D]=eig (covariancen)

k=corrcoef(X)

Coeff =pca(X)

transformed=X*coeff

imagepc1=reshape(transformed(:,1),size(image,1),(size(image,2)));

imagepc2=reshape(transformed(:,2),size(image,1),(size(image,2)));

imagepc3=reshape(transformed(:,3),size(image,1),(size(image,2)));

imagepc4=reshape(transformed(:,4),size(image,1),(size(image,2)));

imagepc5=reshape(transformed(:,5),size(image,1),(size(image,2)));

imagepc6=reshape(transformed(:,6),size(image,1),(size(image,2)));

imagepc7=reshape(transformed(:,7),size(image,1),(size(image,2)));

Figure, imshow (imagepc1, [])

title ('PCA 1')

Figure, imshow (imagepc2, [])
```

title ('PCA 2')

Figure, imshow (-imagepc3, [])

title ('PCA 3')

Figure, imshow (imagepc4, [])

title ('PCA 4')

Figure, imshow (imagepc5, [])

title ('PCA 5')

Figure, imshow (imagepc6, [])

title ('PCA 6')

Figure, imshow (imagepc7, [])

title ('PCA 7')

[COEFF, latent, explained] = pcacov(X)

mapcaplot(X)

Figure, imshow (pca(X))

Matlab scripts for Crosta techniques for alteration of mineral zones
Image=double (imread ('C: \Program Files\MATLAB\LANDSAT IMAGES\mrimanew.tif'));

X = reshape (image, [], 4); s1=std2(X)

v1=var(X (:))

Covariancen=cov(X)

[V, D]=eig (covariancen)

k=corrcoef(X)

Coeff =pca(X)

Transformed=X*coeff

```
imagepc1=reshape(transformed(:,1),size(image,1),(size(image,2)));

imagepc2=reshape(transformed(:,2),size(image,1),(size(image,2)));

imagepc3=reshape(transformed(:,3),size(image,1),(size(image,2)));

imagepc4=reshape(transformed(:,3),size(image,1),(size(image,2)));

Figure, imshow (imagepc1, [])

title ('PCA 1')

Figure, imshow (imagepc2, [])

title ('PCA 2')

Figure, imshow (imagepc3, [])

title ('PCA 3')

Figure, imshow (imagepc4, [])

title ('PCA 4')

FCCimage = cat (3, imagepc1, imagepc2, imagepc4)

Figure

Imshow (FCCimage)

[COEFF, latent, explained] = pcacov(X)
```

List of definitions of terminologies

Absorption band-A range of wavelength in the electromagnetic spectrum within which radiant energy is absorbed by a substance

Albedo- The earth's albedo is a measure of how much incident radiation is reflected

False color- A color imaging process which produces an image that does not correspond to the true color of the scene.

Geographic information system- A combination of mutually referring data sets of various kinds of position and the necessary software to visualize this database.

Image enhancement- The improvements of image to facilitate better information or further digital processing o develop a specific theme or to highlight certain features in an image.

Multispectral-In remote sensing the term implies two or more broad spectral bands in which a sensor detects radiation.

Pixel size- Refers to the dimension of one detector pixel of an array.

Preprocessing- Commonly used to describe the correction and processing of sensor data prior to information extraction.

Radioactivity- It is an effect exhibited by certain types of matter of emitting energy and subatomic particles spontaneously.

Reflectance- Refers to the fraction of the total radiant flux incident upon a surface that is reflected.

Spatial resolution- Defines the minimum separation between two measurements in order for a sensor to be able to discriminate between them.

Spectral resolution- Refers to the resolving power of a system in terms of wavelength.

Radiometric resolution –Refers to the resolving power of a system in terms of the signal energy, intensity and power.

Spectral signature- The response of electromagnetic radiation to particular object in the target area.

Swath- Width of the imaged scene in the spectral direction.

Vegetation index- A mathematical algorithm of reflection values in different spectral bands, used to estimate vegetation characteristics.

Vidicon –A generic name for a camera tube of normal light sensitivity.